(13)

SOURCE DEPTHS UTILIZING BROAD BAND DATA

George H. Sutton, Jerry A. Carter and Noel Barstow
Rondout Associates, Incorporated
P.O. Box 224
Stone Ridge, New York 12484

APRIL 1986

ANNUAL TECHNICAL REPORT
ARPA ORDER NO: 4435
CONTRACT: F08606-85-C-0029

Prepared for:
DEFENSE ADVANCED RESEARCH PROJECTS AGENCY (DARPA)
1400 Wilson Boulevard
Arlington, VA 22209

Monitored by:
AFTAC/TGR
PATRICK AFB
FLORIDA 32925-6001

The views and conclusions contained in this document are those of the authors and should not be interpreted as representing the official policies, either expressed or implied, of the Defense Advanced Research Projects Agency or the United States Government.

UNCLASSIFIED

SECURITY CLASSIFICATION OF THIS PAGE

ADA176010

REPORT DOCUMENTATION PAGE

1a. REPORT SECURITY CLASSIFICATION Unclassified	1b. RESTRICTIVE MARKINGS
2a. SECURITY CLASSIFICATION AUTHORITY	3. DISTRIBUTION/AVAILABILITY OF REPORT Approved for public release; distribution is unlimited.
2b. DECLASSIFICATION/DOWNGRADING SCHEDULE	
4. PERFORMING ORGANIZATION REPORT NUMBER(S)	5. MONITORING ORGANIZATION REPORT NUMBER(S)
6a. NAME OF PERFORMING ORGANIZATION Rondout Associates, Inc. 6b. OFFICE SYMBOL (If applicable)	7a. NAME OF MONITORING ORGANIZATION AFTAC/TGR
6c. ADDRESS (City, State and ZIP Code) P.O. Box 224 Stone Ridge, New York 12484	7b. ADDRESS (City, State and ZIP Code) Patrick Air Force Base Florida 32925-6001
8a. NAME OF FUNDING/SPONSORING ORGANIZATION DARPA 8b. OFFICE SYMBOL (If applicable) GSD	9. PROCUREMENT INSTRUMENT IDENTIFICATION NUMBER
8c. ADDRESS (City, State and ZIP Code) 1400 Wilson Boulevard Arlington, Virginia 22209	10. SOURCE OF FUNDING NOS. PROGRAM ELEMENT NO.: 62714 E PROJECT NO.: DT/5126 TASK NO.: A11 WORK UNIT NO.: 6A10
11. TITLE (Include Security Classification) Source Depths Utilizing Broad Band Data	
12. PERSONAL AUTHOR(S) George H. Sutton, PI, Jerry A. Carter, Noel Barstow	
13a. TYPE OF REPORT Annual Technical 13b. TIME COVERED FROM 11Apr85 TO 10Apr86	14. DATE OF REPORT (Yr., Mo., Day) 11 April 1986 15. PAGE COUNT 51
16. SUPPLEMENTARY NOTATION	

17. COSATI CODES		
FIELD	GROUP	SUB. GR.
8	11	
17	10	

18. SUBJECT TERMS (Continue on reverse if necessary and identify by block number)
depth determination, polarization filtering, state filtering, comparison with synthetic seismograms, three-component data, earthquakes in northeastern North America

19. ABSTRACT (Continue on reverse if necessary and identify by block number)

This report covers the first year's effort of a two year research project to improve our ability to discriminate between nuclear explosions and earthquakes based on the depth of an event determined from local and regional phases. The approach taken has been to improve phase identification and picking abilities for depth phases pP and sP through adaptive filtering to reduce effects of mode conversion and scattering. Three-component polarization methods are applied to broad-band digital data from a set of earthquakes located in the northeastern United States and adjacent Canada. The "cleaned up" data are compared with suites of synthetic seismograms for different depths and focal mechanisms obtained using two velocity/attenuation models appropriate for northeastern United States and Canada. This comparison provides a basis for identification of the depth phases and discrimination of other reflected/refracted arrivals in the P wavetrain. Polarization state filtering (following procedures proposed by Samson) is used to emphasize those frequencies exhibiting the desired particle motion within a time window that slides through

20. DISTRIBUTION/AVAILABILITY OF ABSTRACT UNCLASSIFIED/UNLIMITED ☒ SAME AS RPT. ☐ DTIC USERS ☐	21. ABSTRACT SECURITY CLASSIFICATION Unclassified
22a. NAME OF RESPONSIBLE INDIVIDUAL Dr. Dean A. Clauter	22b. TELEPHONE NUMBER (Include Area Code) 305-494-5263 22c. OFFICE SYMBOL AFTAC/TGR

DD FORM 1473, 83 APR EDITION OF 1 JAN 73 IS OBSOLETE.

UNCLASSIFIED

SECURITY CLASSIFICATION OF THIS PAGE

the P wavetrain. Adaptive orientation of the state filtered data into radial and transverse horizontal components and determination of azimuths and apparent angles of incidence further facilitates phase identification and comparison with synthetics. Eight local and regional earthquakes and one quarry blast were selected for study. Polarization filtering reduces much of the P coda and emphasizes discrete portions of the wavetrain as anticipated. In most cases, detailed phase identification and comparison with synthetics has not yet been made. Detailed comparison of the "cleaned up" P wavetrain for the Gaza, New Hampshire earthquake of 19 January 1982 with a suite of synthetics illustrates the capabilities and limitations of the procedures developed to date. Apparent fits are obtained at depths of 4.5 and 9 kilometers (km) as well as at the preferred depth of 6 km. (Previous workers obtained estimates for this earthquake between 3 and 11 km using various regional, teleseismic and network methods.)

TABLE OF CONTENTS

LIST OF ILLUSTRATIONS

SECTION I

INTRODUCTION

The purpose of the research presented in this document is to refine our ability to discriminate between nuclear explosions and earthquakes based on the depth of an event determined from local and regional phases. If the depths of seismic events can be determined accurately, many events can be eliminated as potential nuclear explosions based on the practical limit of nuclear explosion burial depth. This discriminant has been used for many years at teleseismic distances. The higher frequency data obtained at local and regional distances improves the depth resolution of the method and thus the minimum depth at which the discriminant may be applied. In addition, smaller events not recorded at teleseismic distances may be seen at regional and/or local distances.

Our approach to this problem has been to improve phase identification and picking abilities of depth phases *pP* and *sP* through filtering and three-component polarization methods. These methods are applied to data from a set of earthquakes located in the northeastern United States and adjacent Canada. The area of study was chosen for several reasons:

(1) the large majority of events in this area occur at depths less than 15 km so that a data set of shallow events is readily available,

(2) the geology and tectonic setting of the area is well known and similar to that found in the Soviet Union,

(3) the depths of the events in the area of study are fairly well known from network studies and aftershock surveys, and

(4) there are broad-band three-component digital seismic stations in the immediate vicinity (RSNY and SRNY).

The most difficult problem associated with depth determination at local and regional distances using depth phases is identification. As the depth phases are usually buried in the coda, data processing plays a key role in identifying and picking them. Band-pass filtering and three-component polarization state filtering methods are used on the data in an attempt to isolate the depth phases and adaptive polarization analysis is used to help identify them.

Once the depth phases have been correctly identified and picked, the depth can be determined accurately if the source region velocity structure is known. However, misidentification of phases and inaccurate time picks can lead to severe errors in the depth estimates. To assess the potential depth errors resulting from these problems, synthetic seismogram depth sections have been generated for each of the events to compare to the identification and time picks made from the data. Of course, the depth of the event is not the only factor contributing to the character of the depth section; the velocity-depth structure used and the focal mechanism are also very important to the overall character of the section.

This report covers the first year's effort of a two year research project. In the sections that follow, we briefly describe the analysis methods used on the data to isolate depth phases, review the set of earthquakes that we have selected for study, present the synthetic seismograms for these events, and show a detailed analysis of the January 19, New Hampshire earthquake.

SECTION II

POLARIZATION ANALYSIS METHODS

Polarization analysis of a three-component wavefield is used to determine the vector particle motion characteristics such as the degree of polarization, direction of propagation and ellipticity. This information can then be used to design filters that emphasize or eliminate waves having specific polarization properties. In seismology, this method has been applied to analyze and filter waves coming from certain directions, or having rectilinear or elliptical particle motion, and to discriminate against isotropic noise (Sutton and Pomeroy, 1963; White, 1964; Archambeau et al., 1965) .

Polarized arrivals can be enhanced, their wave type identified, and their direction of propagation, as well as their phase velocity for body waves and ellipticity for Rayleigh waves, determined. This information can then be used for phase identification, epicentral location, source depth determination, earth structure studies, ...etc. Data filtered for polarized signal are more amenable to comparison with synthetic seismograms, providing a better determination of relevant parameters.

The polarization state method was proposed by Samson (1977) for the analysis and filtering of seismograms. It makes use of the spectral matrix, which is the frequency domain equivalent of the cross-correlation matrix of the data, smoothed over a frequency window. Various spectral estimators can be obtained from the spectral matrix, such as the degree of polarization, the degree of rectilinear polarization, a detector for signal in a specific "pure state" (i.e. completely polarized) or with specific polarization characteristics. Such estimators can then be used to filter the data in order to discriminate against unpolarized noise or to enhance signal in some specific polarization state (Samson and Olson, 1981). Since the polarization characteristics of seismograms continuously change with time, such filters have to be data-adaptive: a sliding time window of data is analyzed and a filter is specifically designed for that window. Polarization properties are determined and used not only as a function of time, but also as a function of frequency, since the processing is done in the frequency domain. This is an advantage that methods which operate purely in the time domain do not have.

To enhance depth phases *pP* and *sP* we take advantage of the three-component polarization state filter's ability to pass frequencies that contain rectilinearily polarized motion and reject frequencies that do not.

After the data have been state filtered for rectilinear motion, they are processed with an adaptive polarization method. The horizontal components are adaptively rotated to the time varying radial and transverse directions and the time variable azimuth and apparent angle of incidence are given. This process helps in the identification of phases. Also, the synthetic seismogram components are the radial and vertical so rotating the horizontal data to the adaptive radial and transverse components facilitates comparison.

The polarization state filter and the adaptive polarization process form the core of the data processing for this project.

SECTION III

NORTHEAST EVENTS

Eight local and regional earthquakes and one quarry blast were selected for comparison with synthetic seismograms discussed below. The events were chosen for their size, location, and availability of data. A list of these events is given in Table 1 along with location, depth, magnitude, strike, dip, and rake of the focal mechanism, the region (either New England or Grenville), and references for the focal parameters. The event and station locations are plotted in Figure 1, showing their spatial distribution. Many of the earthquakes in Table 1 have been studied by others and, for some, the focal depths and focal mechanisms are well determined and will enable us to test the methods we are developing.

In addition to reviewing the literature, we examined phase data from local seismic networks originally used to invert for hypocentral location. In three cases the estimated error on focal depth was so large that to use the reported depth would be misleading. For these we indicate (Table 1) an unknown depth.

Figures 2A through 2I, all in essentially the same format, show the three-component seismograms for events in Figure 1. Most were recorded by the Regional Seismic Test Network (RSTN) station, RSNY, in northern New York and several of the recent events have been recorded by SRNY, a very-broad-band seismic station operated by Rondout Associates in Stone Ridge, New York. Just the *P*-wave portion of the seismograms is shown in these figures since depth phases are our primary interest. As mentioned in the introduction, one of the keys to understanding the data and being able to compare them to synthetic seismograms will be the extraction of discrete phase arrivals from the *P*-coda waves. Along with the unfiltered or high-pass filtered data (the top three traces in figures 2A through 2I), we present three-component state filtering of the data (the bottom three traces). These are filtered to pass rectilinear particle motion as a function of both frequency and time (as described in analysis methods above). In all cases, polarization-state filtering serves to enhance some portions of the seismograms relative to other portions. We are currently investigating ways of identifying the phases in these "cleaned up" seismograms. An example, the January 19, 1982 New Hampshire earthquake, is presented following the discussion of synthetic seismograms.

TABLE 1. LIST OF EVENTS AND EVENT PARAMETERS

Date	Time	Lat	Lon	Depth	M	Strike	Dip	Rake	Reg	Refs
Jan 19, 1982	00:14:42.00	43.49	-71.59	3 - 11	4.5 M_b	280	75	-11	NE	1,2,3,4
Aug 31, 1982	10:16:58.10	43.21	-74.20	?	2.6 M_n	173	60	110*	C	1,5
May 29, 1983	05:45:49.80	44.50	-70.41	2	4.2 M_b	355	52	78	NE	1,6
Oct 07, 1983	10:18:46.10	43.94	-74.26	7-12	5.2 M_b	173	60	110	C	1,5,7,8,9
Oct 11, 1983	04:10:55.00	45.21	-75.77	12	4.1 M_{bLg}	071	75	98	C	1,10
Oct 23, 1984	06:26:21.71	43.59	-73.94	?	3.4 M_c	173	60	110*	C	1,5
Oct 02, 1985	21:10:07.00	42.90	-74.14	0	2.3 M_c	Chem	Ex		App(NE)	
Oct 19, 1985	10:07:40.30	40.98	-73.83	5	4.0 M_L	022	90	180	App(NE)	1,11
Oct 30, 1985	03:42:48.60	42.93	-74.11	?	2.7 M_{bLg}	018	60	156**	App(NE)	1,12

* Generic Adirondack Fault Plane Solution (from 7)
** Generic Mid-Hudson Fault Plane Solution (from 12)

References:

1. Preliminary Determination of Epicenters
2. Pulli et al., 1983
3. Brown and Ebel, 1985
4. Barstow et al., 1986
5. Regional Seismicity Bulletin of Lamont-Doherty Seismic Network
6. Ebel and McCaffrey, 1984
7. Suarez et al., 1984
8. Seeber et al., 1984a
9. Seeber et al., 1984b
10. Wahstrom, 1983
11. Seeber et al., 1986
12. Houlday et al., 1984

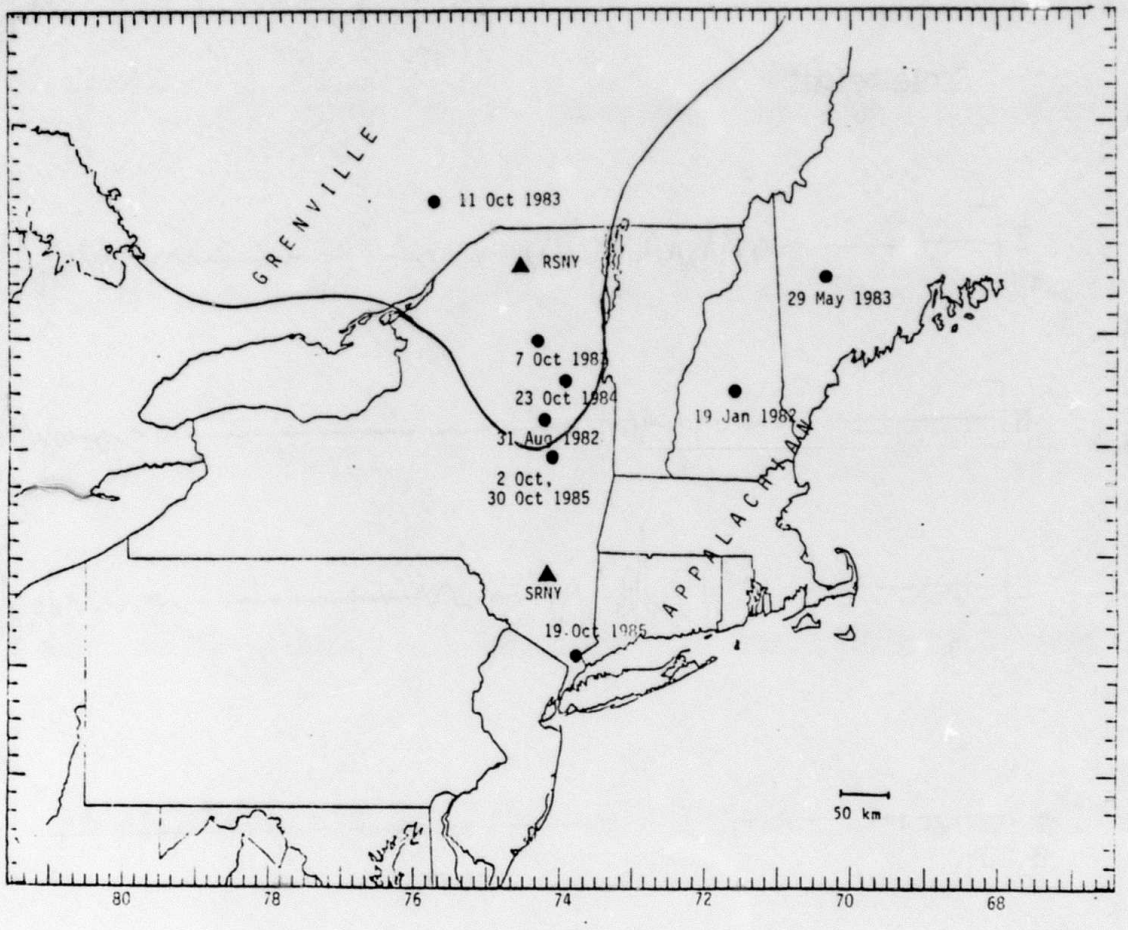

Figure 1. Location of events and stations used in this study. Events are indicated by circles and a date. The two stations, RSNY and SRNY are indicated by triangles.

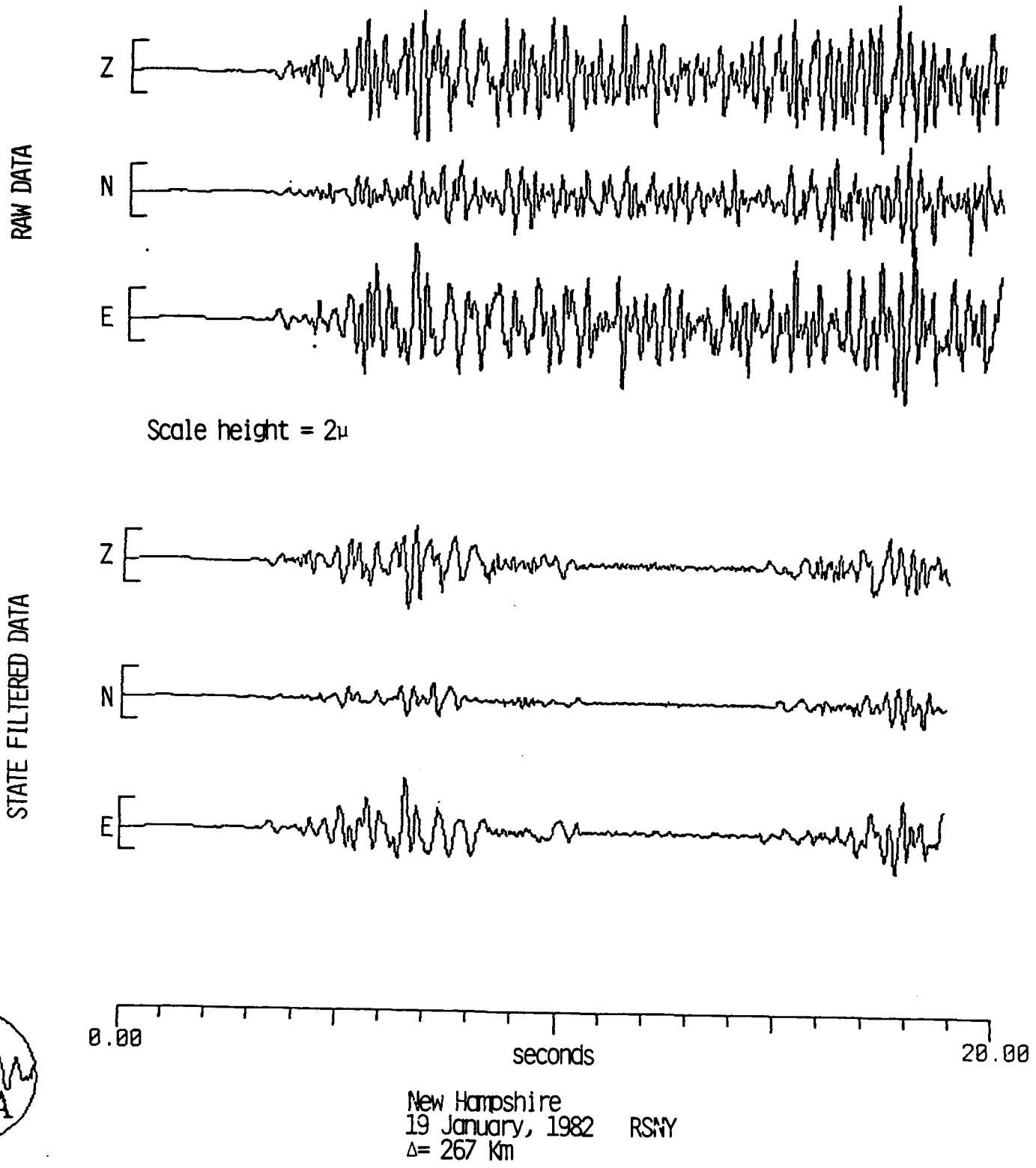

Figure 2A. Seismograms recorded at RSNY of the January 19, 1982, New Hampshire earthquake. The top three traces are the vertical, north-south, and east-west components, unfiltered. The bottom three traces are the three components after state-filtering for rectilinear particle motion. The rest of the events shown in Figure 1 are similarly depicted in Figures 2B through 2I.

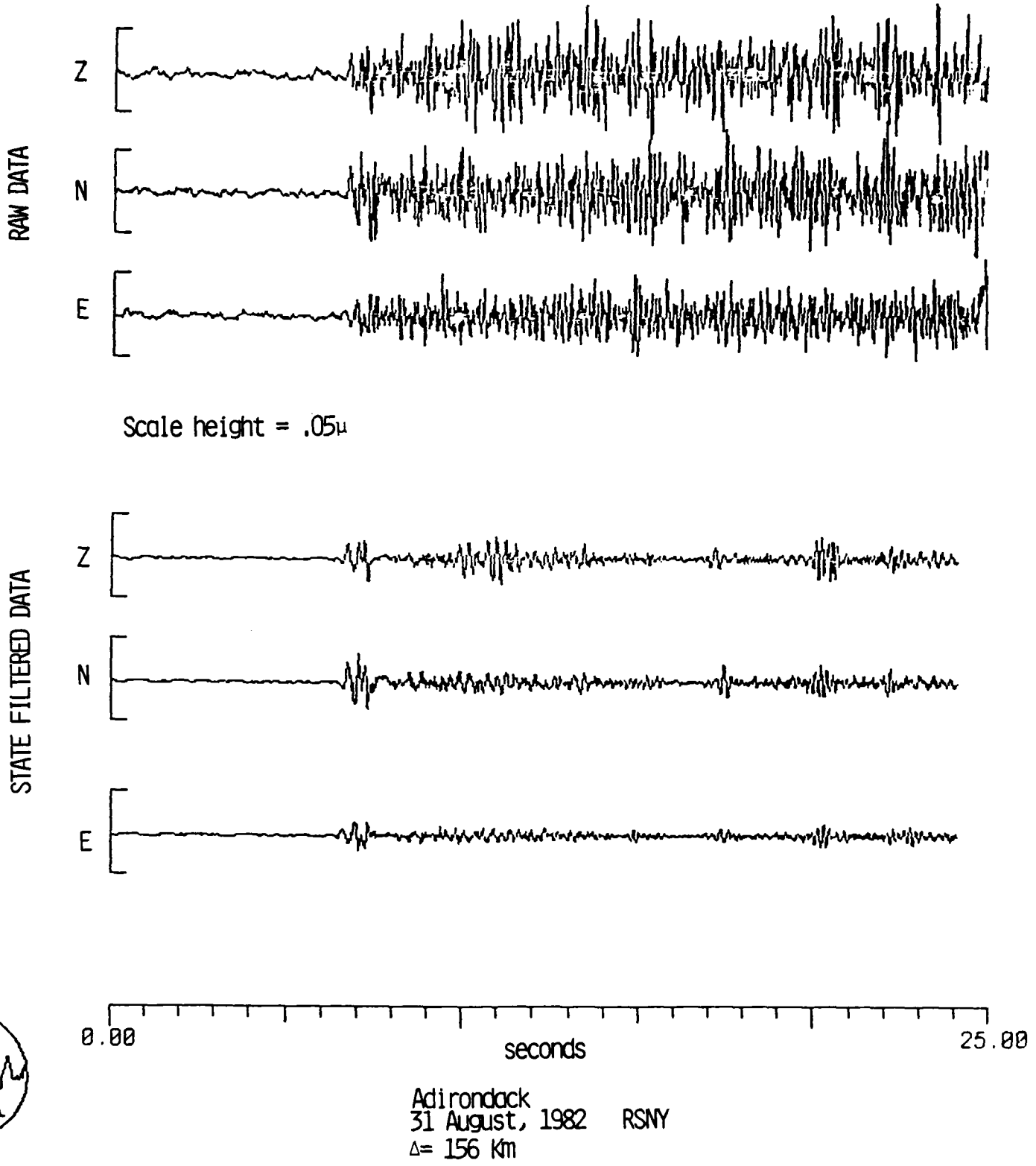

Figure 2B. 31 August Adirondack earthquake.

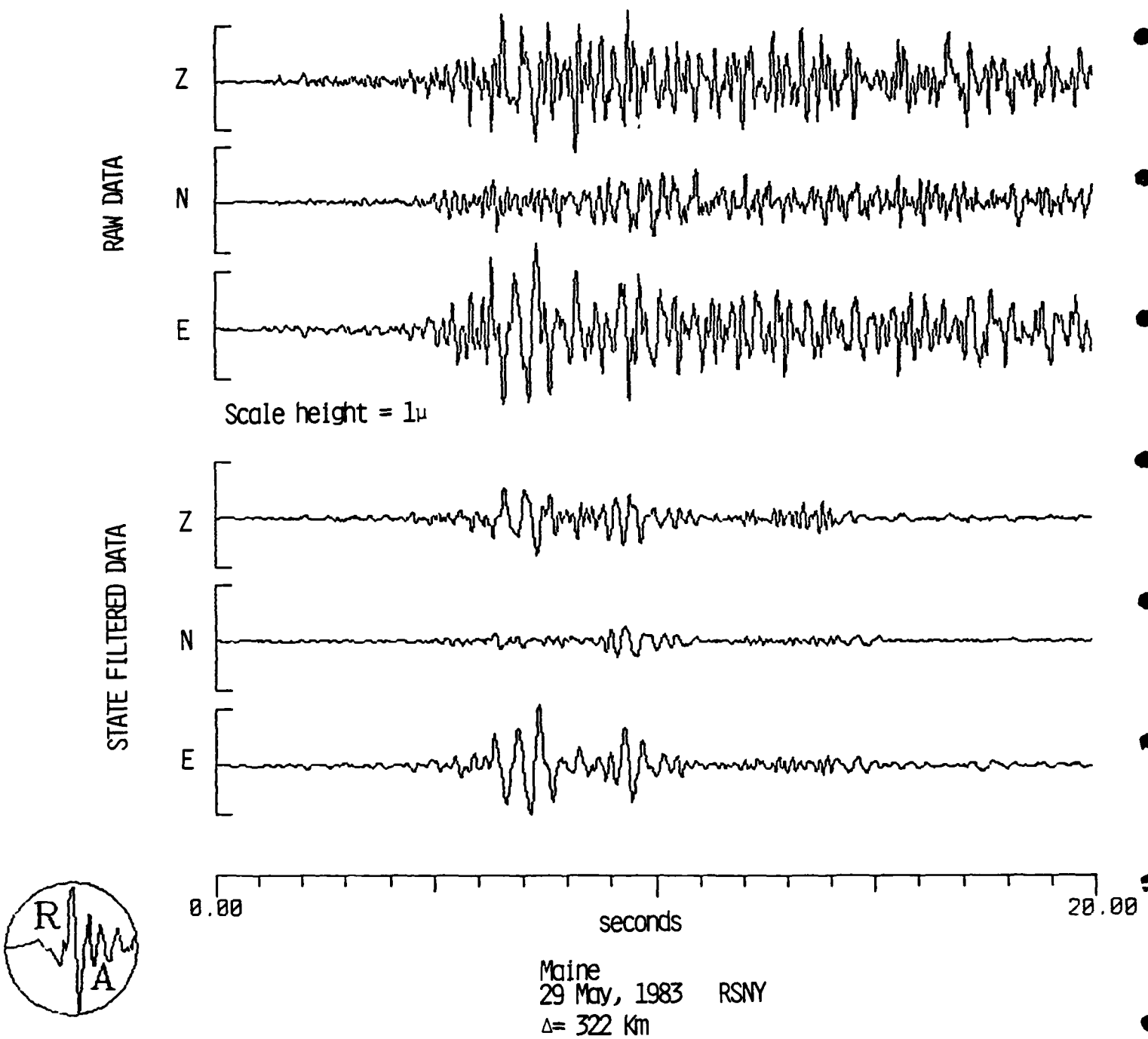

Figure 2C. 29 May 1983 Maine earthquake.

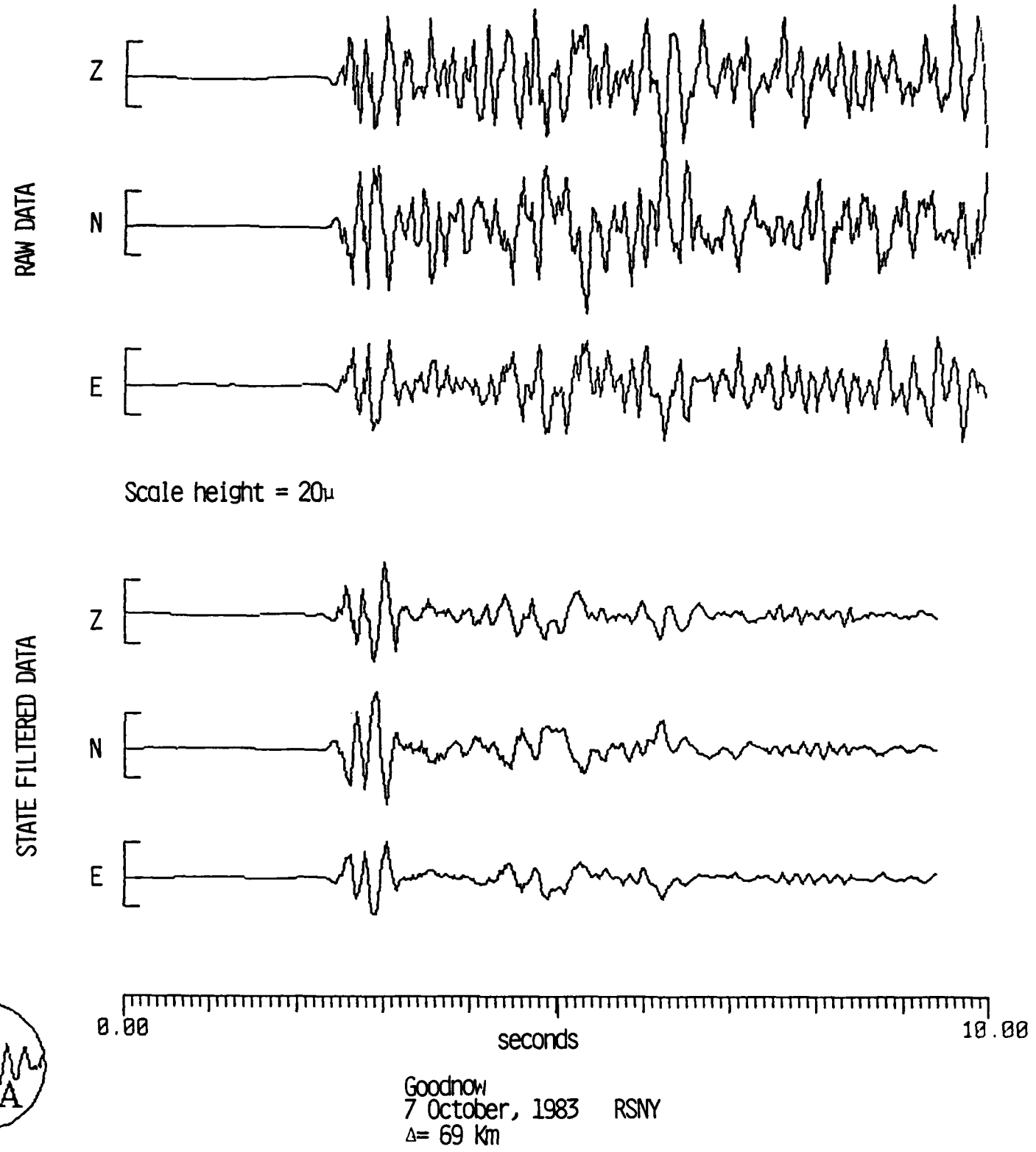

Figure 2D. 7 October 1983 Goodnow earthquake.

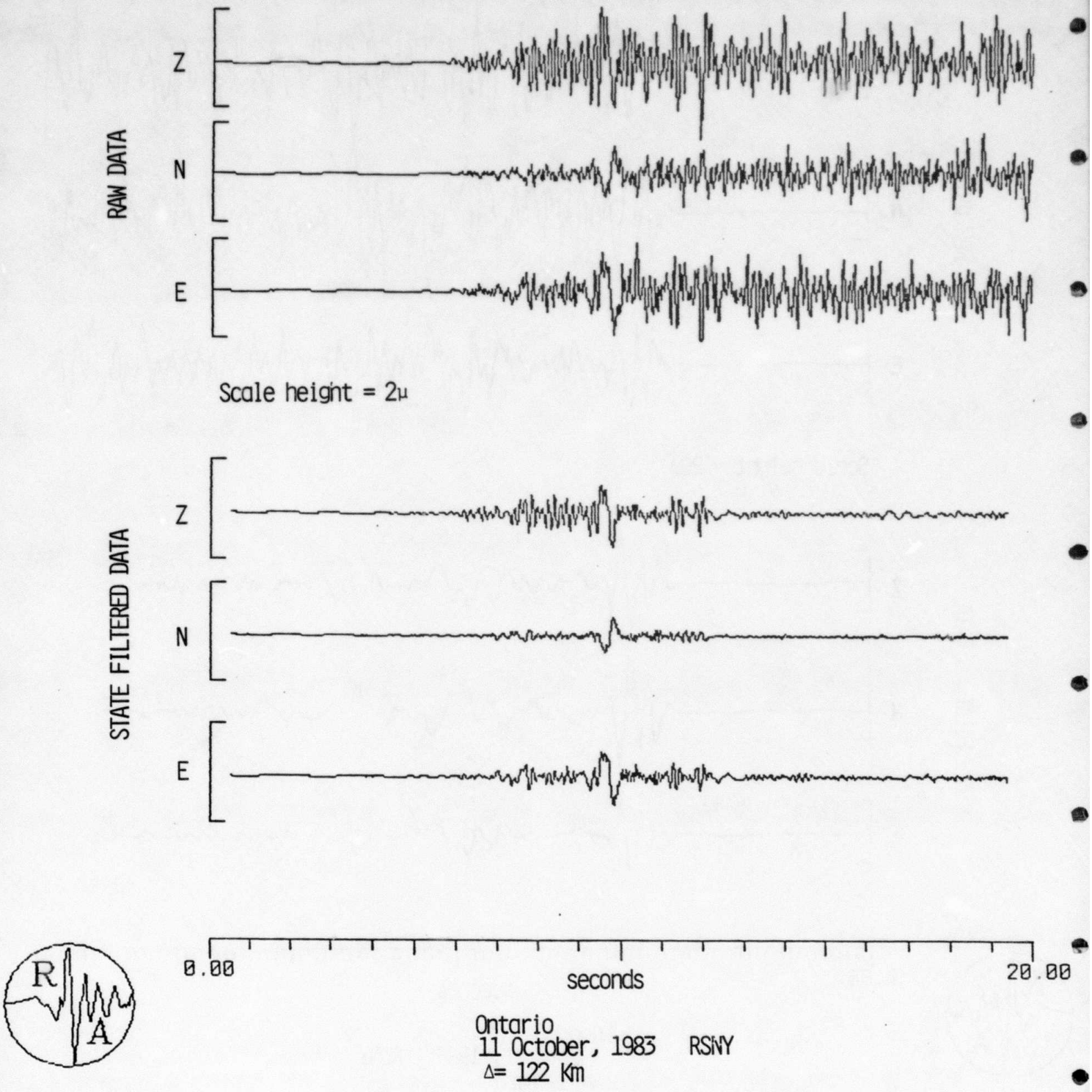

Figure 2E. 11 October 1983 Ontario earthquake.

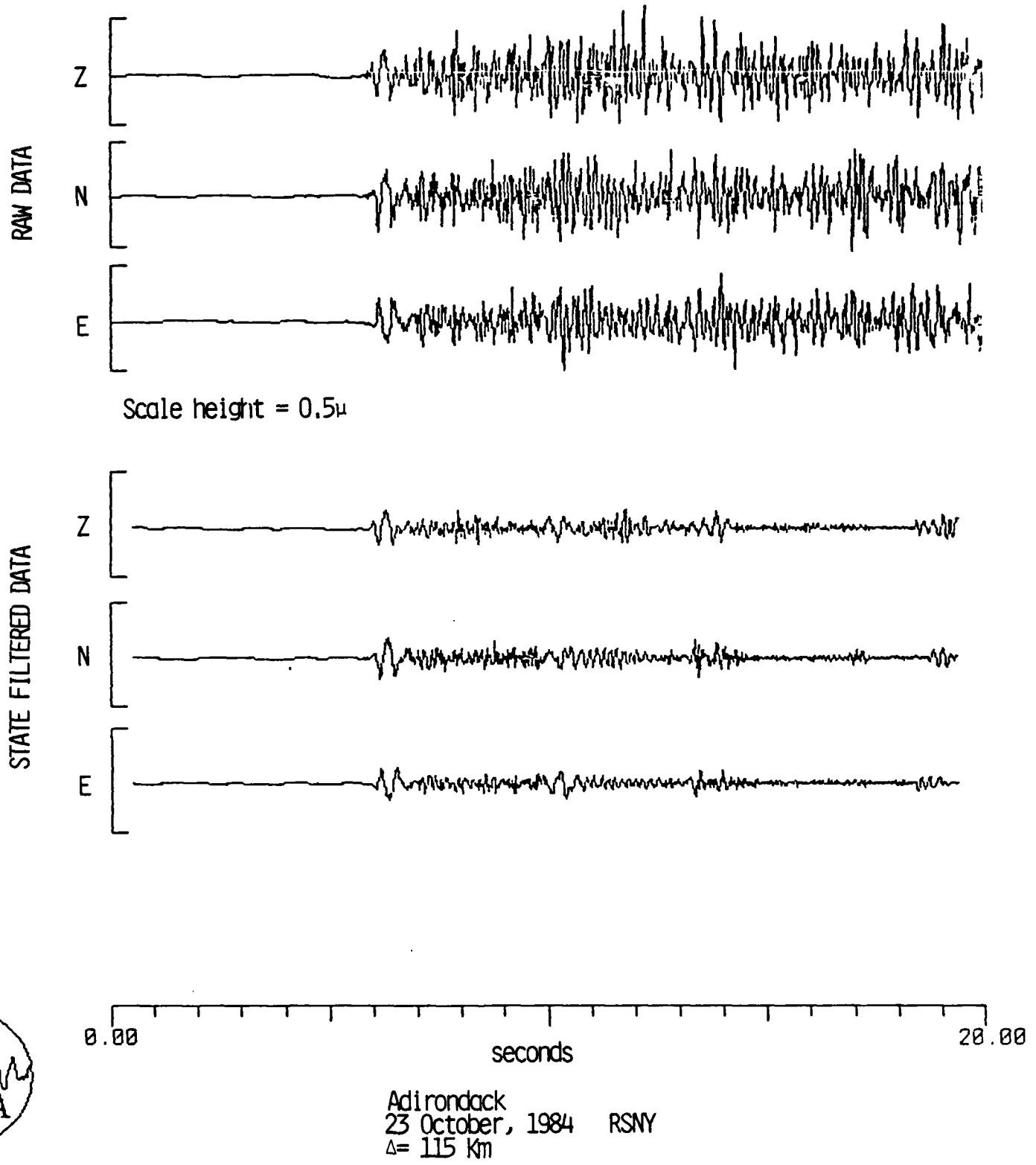

Figure 2F. 23 October 1984 Adirondack earthquake.

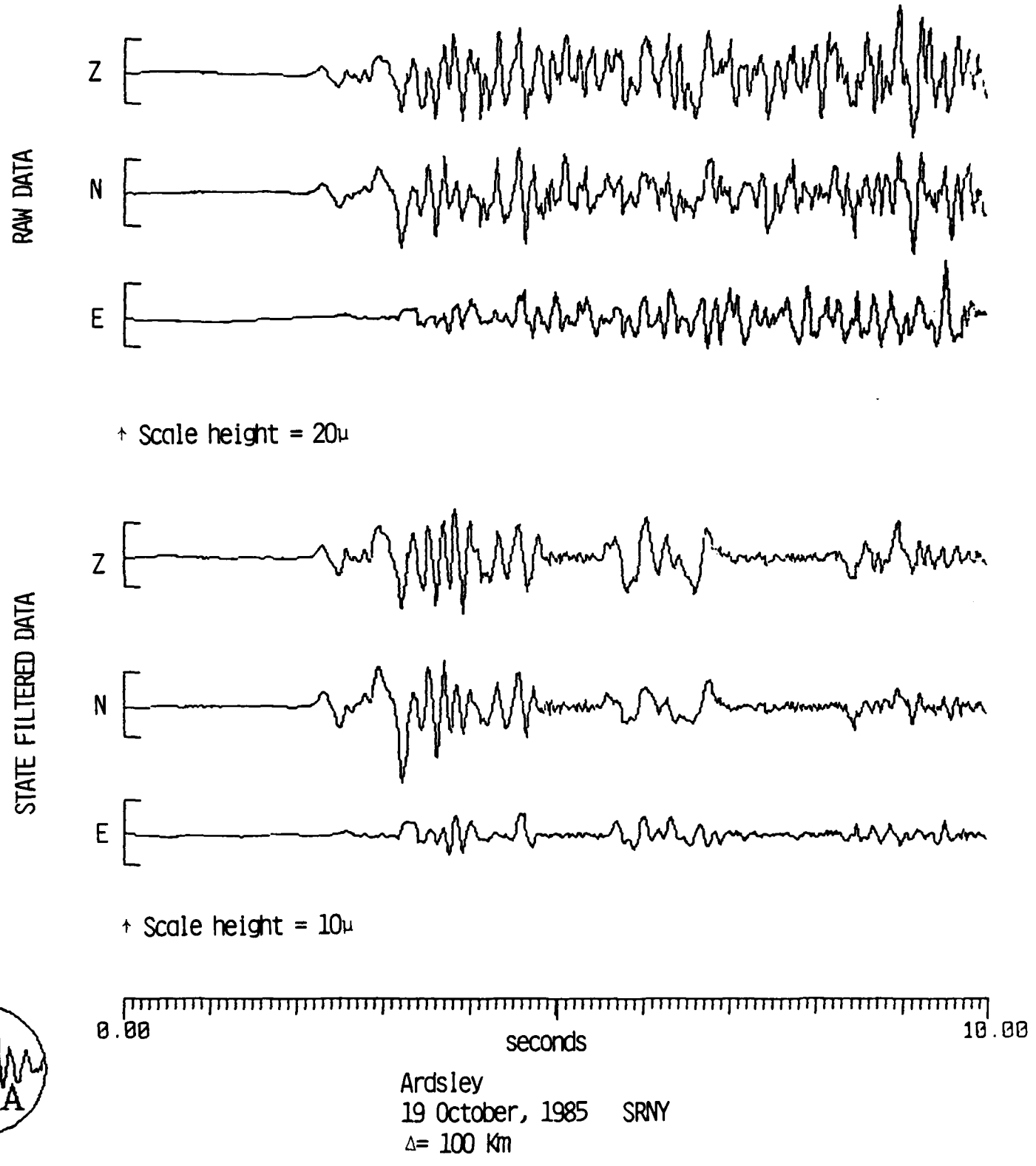

Figure 2G. 19 October 1985 Ardsley earthquake.

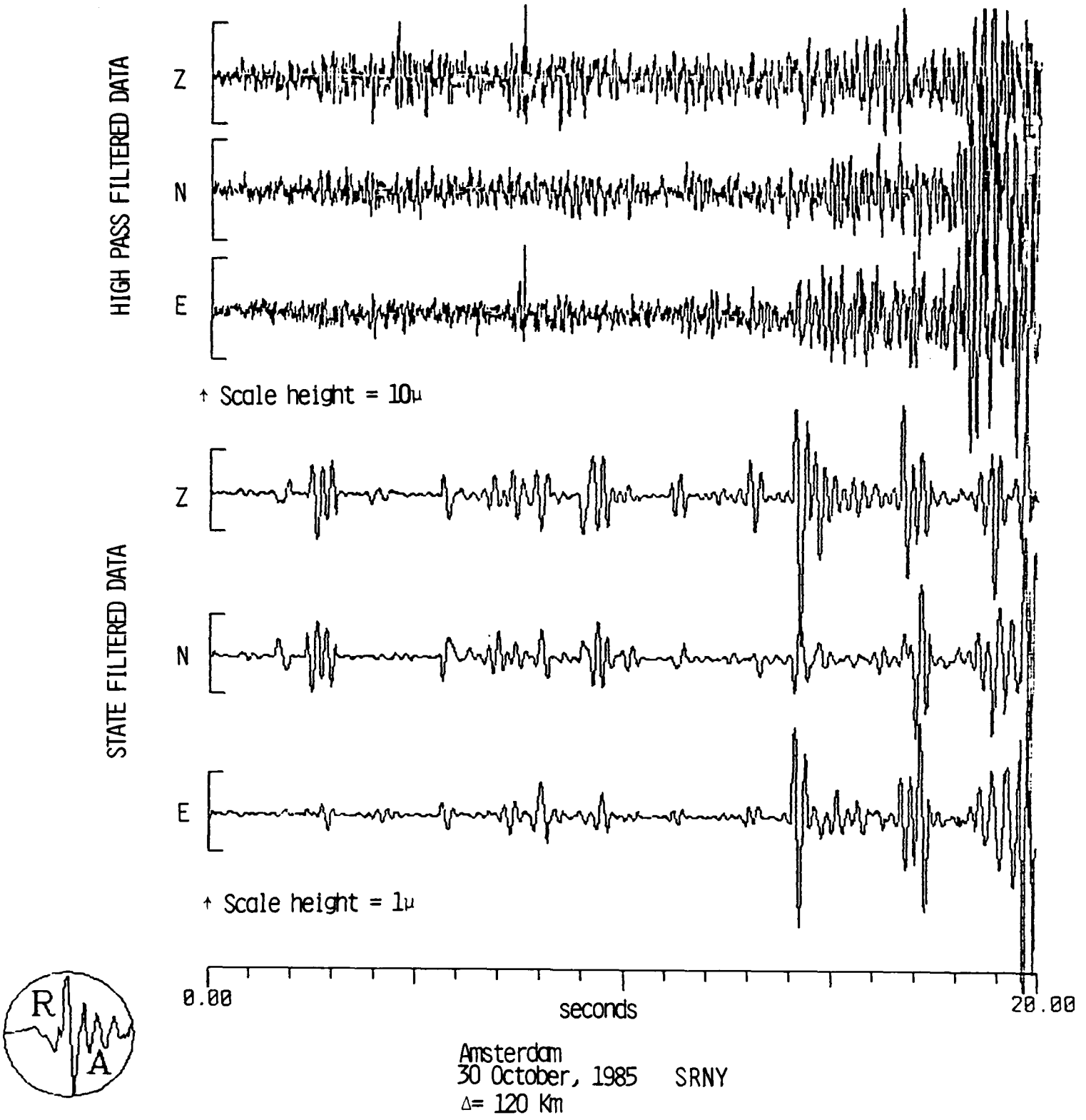

Figure 2H. 30 October 1985 Amsterdam earthquake.

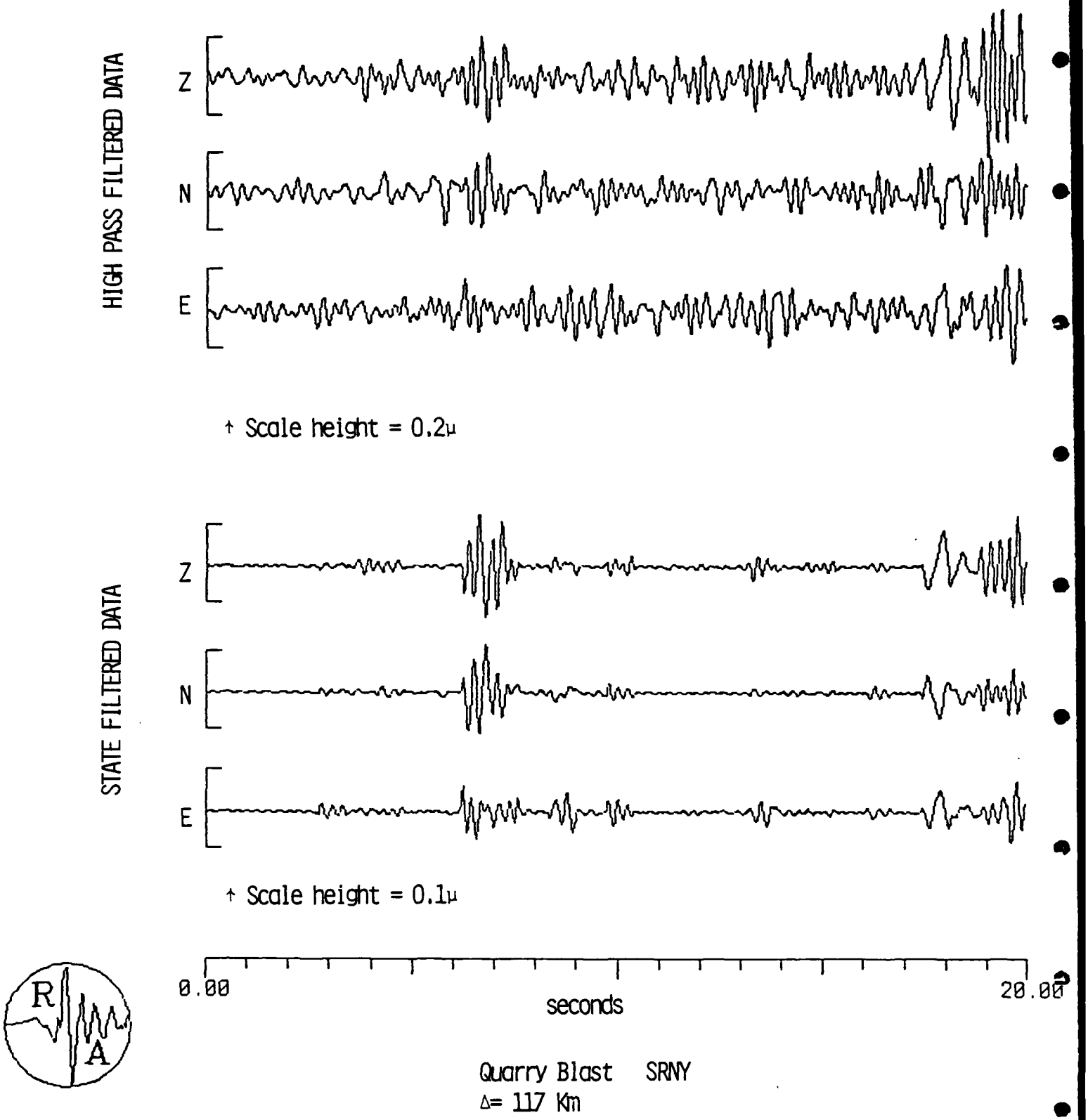

Figure 2I. Quarry Blast

SECTION IV

SYNTHETIC SEISMOGRAMS

The synthetic seismograms were computed using the locked mode method (Harvey, 1981). Frequencies from zero to 5 Hz are computed. Regional geology in the Northeast required that two different velocity/attenuation models be used for the computation; a New England model for the events in New England and southern New York, and a Grenville model for events within the Grenville province (Figure 1, Table 2). The New England velocity model was derived by Taylor et al., (1980) using regional travel times of *P* and *S* waves recorded across the Northeastern United States Seismic Network operated by several academic, governmental and private institutions in the northeast. The Grenville model was from unpublished refraction results. The frequency and depth dependent Q model for the New England model was adapted from work by Mitchell (1981) and a simple frequency dependent Q was used for the Grenville model. Although there are significant differences in the Q models, there is little effect on the synthetics because the frequencies and ranges at which they are being computed are relatively small.

Synthetics were computed for each event at several depths with the reported focal mechanism listed in Table 1. The instrument response was convolved with the synthetics for comparison to the data.

Station RSNY lies within the Grenville structure close to the boundary with the New England Structure. While the travel paths to RSNY from New England events must pass through both structures, the majority of the path is within the New England structure and so the New England structure is a good approximation to the true path.

In Figures 3A through 3H we show the synthetic depth sections for the events in Table 1. Only the first 20 or so seconds are shown as we wish to emphasize the characteristics of the depth phases with focal mechanism, depth, range, and velocity model. Some of the phases are identified in the synthetic sections with labeled lines. Reflections off of the 13 km discontinuity in the New England model and the 4 km discontinuity in the Grenville model are indicated with an "i" (e.g. *PiP*). Mantle reflections are indicated by an "m". The depth phases are characterized by progressively later arrivals with increased depth and the primary phases by either very little change in arrival time with depth for the direct arrivals or progressively earlier arrivals with increased depth. Notice that in some of the sections, the depth phases dominate, while in others, the primary phases dominate. This is a function of the theoretical radiation pattern predicted by the input focal mechanism. Because the input velocity structure will influence the take-off angle of each phase and hence its position on the focal sphere, both focal mechanism and velocity model are contributing to the relative amplitudes of primary and depth phases.

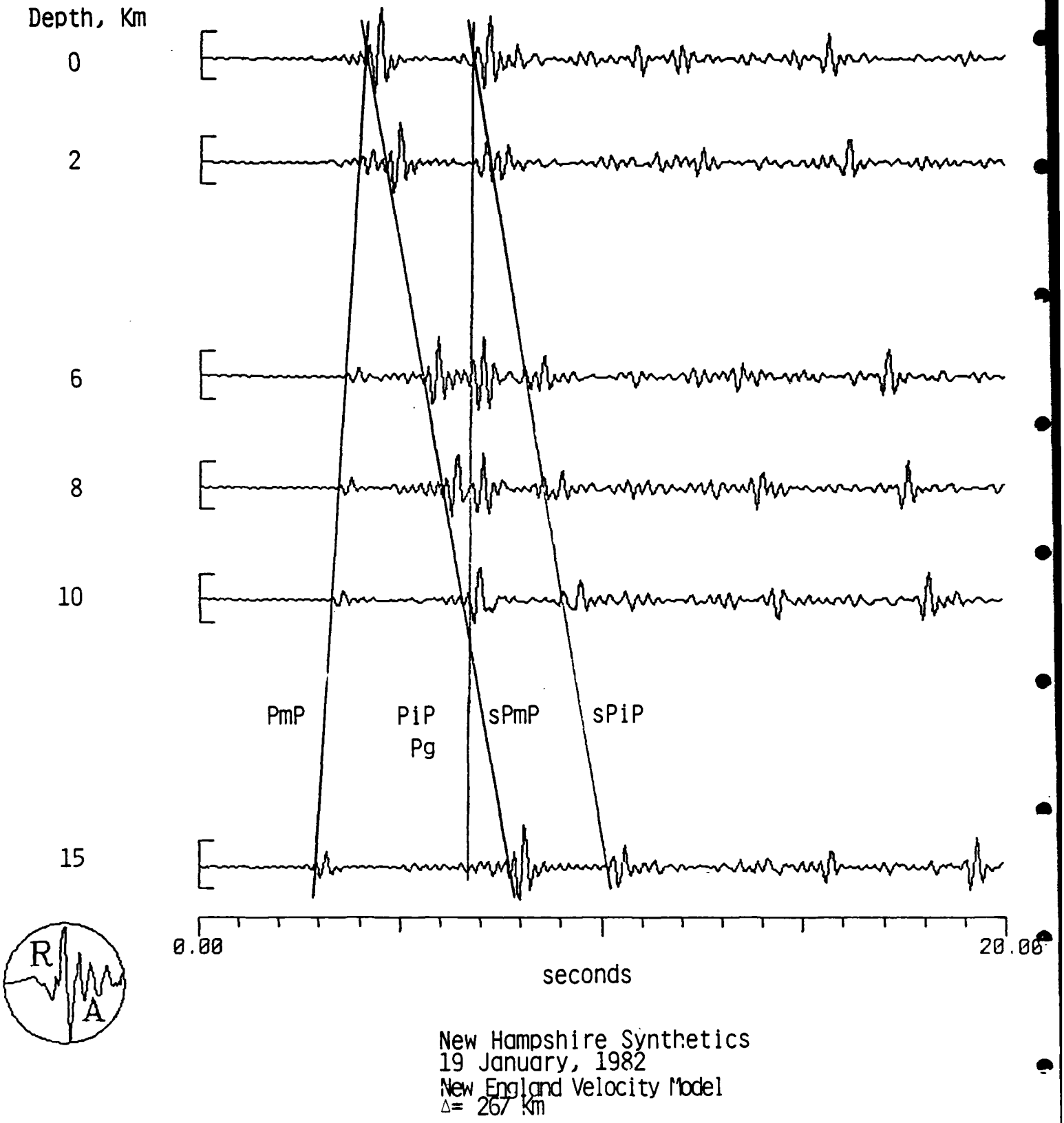

Figure 3A. Synthetic seismograms calculated for a suite of depths. Source= January 19, 1982 Earthquake. Strike= 280, Dip= 75, Rake= -11. Receiver response= RSNY short period (sp). Azimuth=295. In Figures 3A through 3H several primary and depth phases are identified. All but Figure 3G are vertical components.

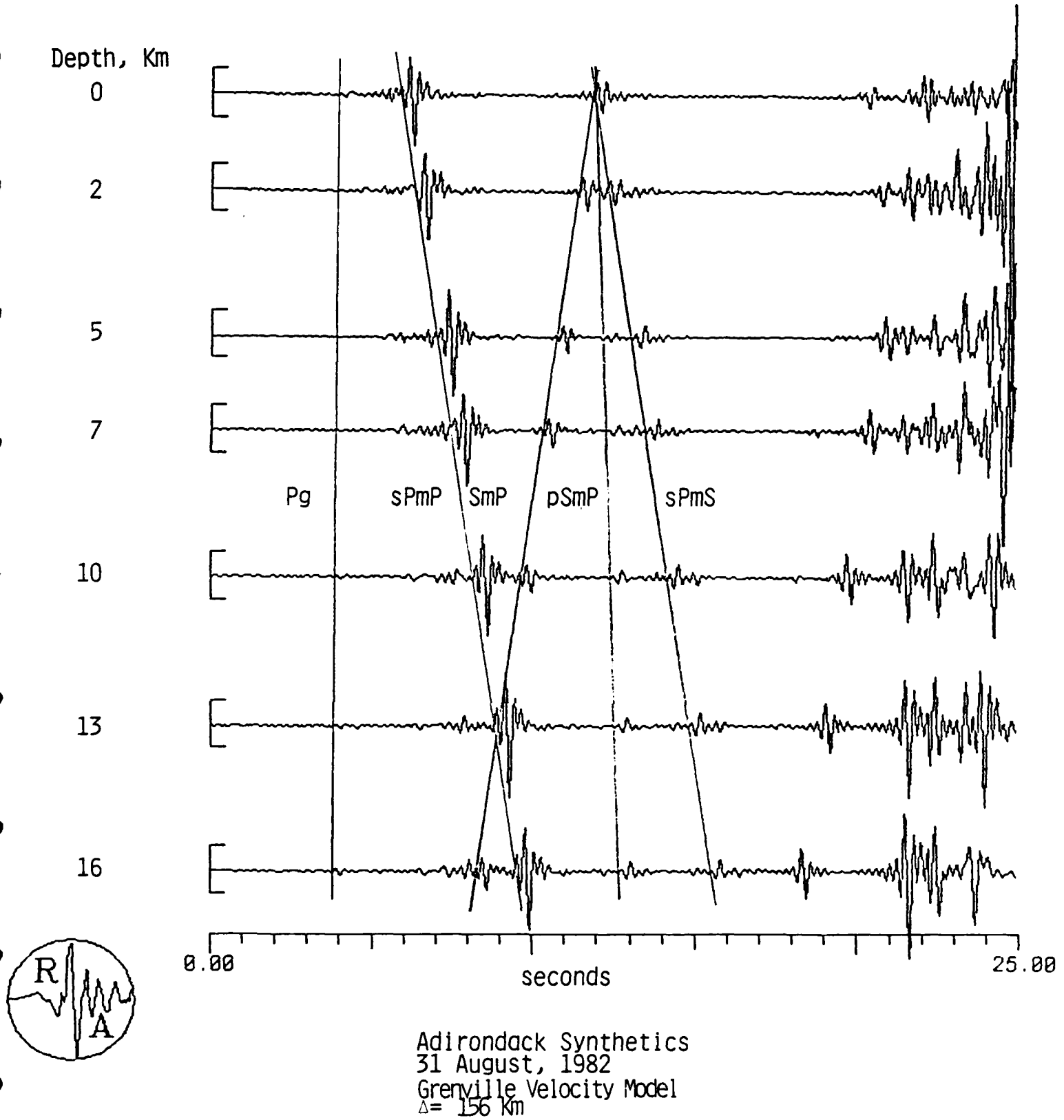

Figure 3B. Synthetic seismogram depth section. Source= 31 August, 1982 Earthquake. Strike= 173, Dip= 60, Rake= 110. Receiver response= RSNY (sp). Azimuth= 350.

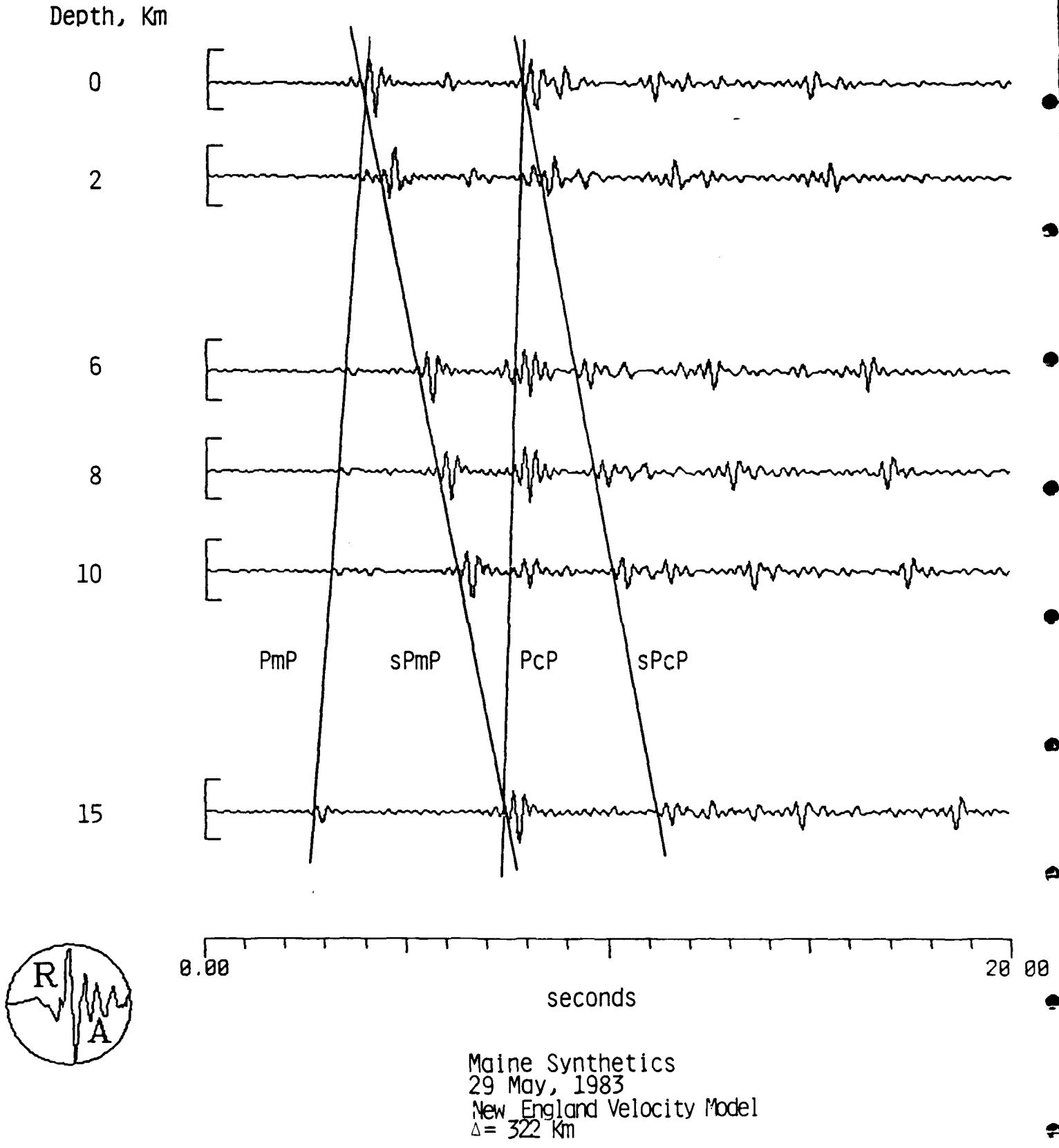

Figure 3C. Synthetic seismogram depth section. Source= 29 May, 1983 Earthquake. Strike= 355, Dip = 52, Rake= 78. Receiver response= RSNY (sp). Azimuth= 269.

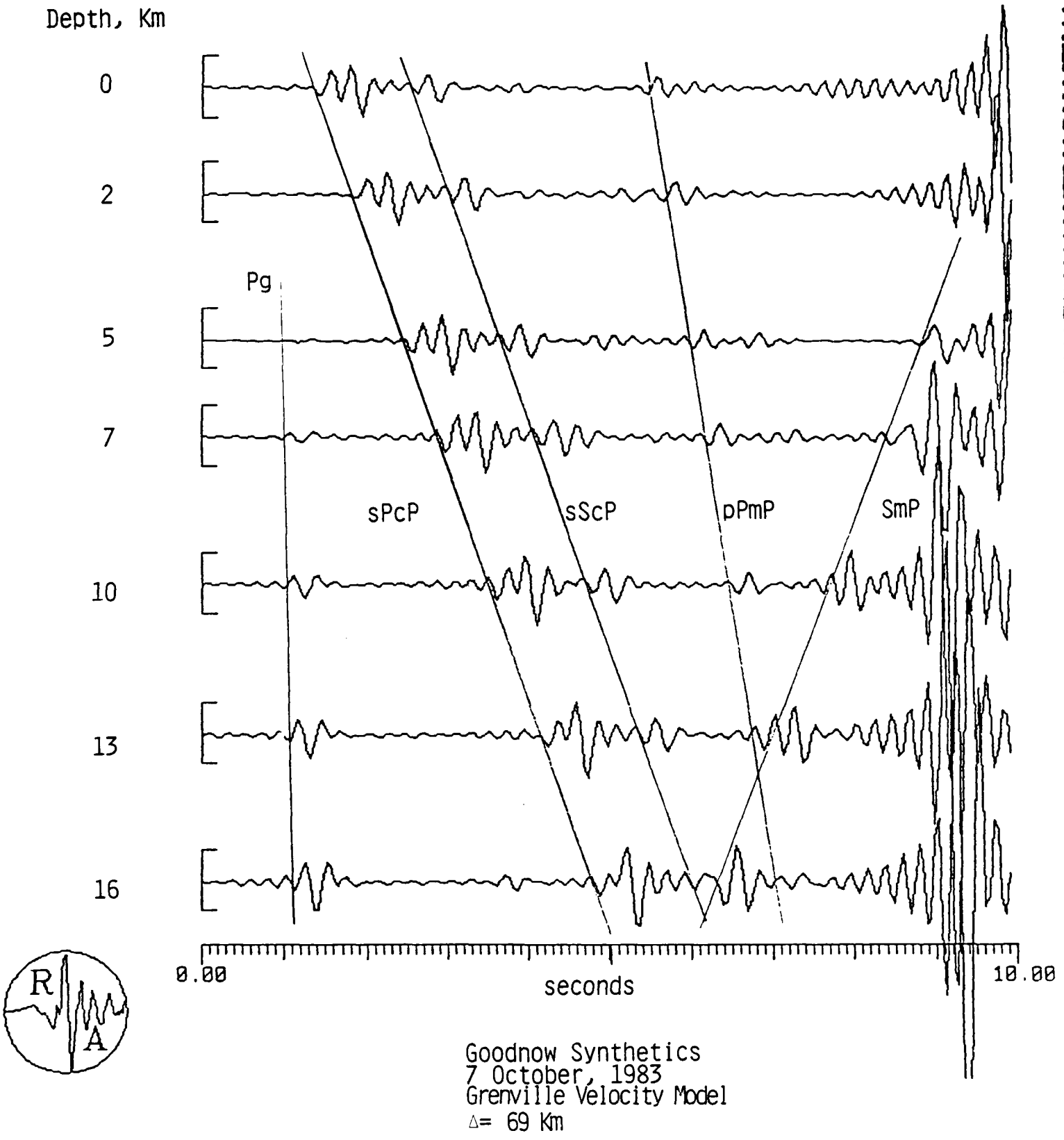

Figure 3D. Synthetic Seismogram depth section. Source= 7 October, 1983 Earthquake. Strike= 173, Dip= 60, Rake= 110. Receiver response= RSNY (sp). Azimuth= 342.

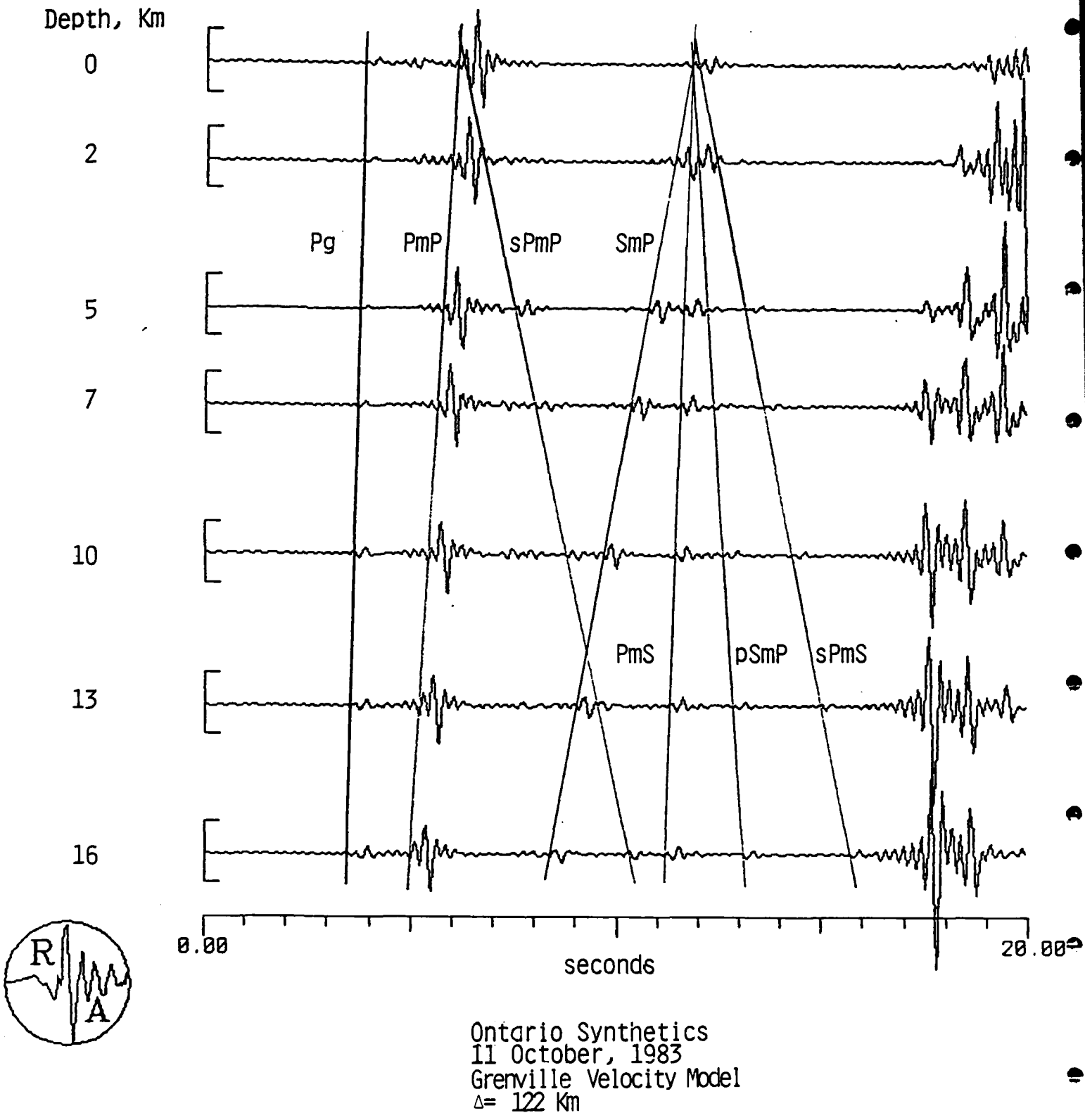

Figure 3E. Synthetic Seismogram depth section. Source= 11 October, 1983 Earthquake. Strike= 71, Dip= 75, Rake= 98. Receiver response= RSNY (sp). Azimuth= 127.

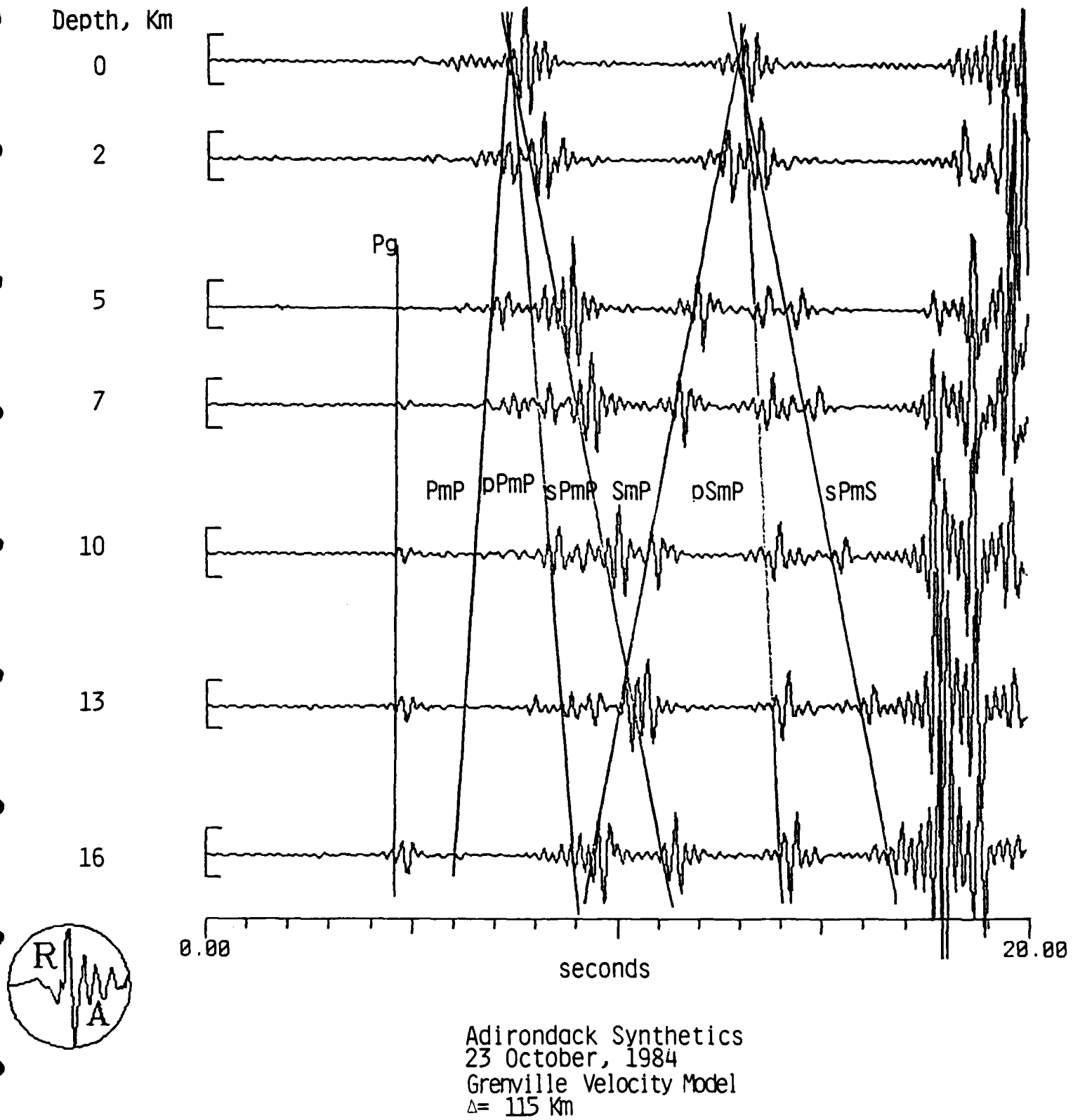

Figure 3F. Synthetic Seismogram depth section. Source= 23 October, 1984 Earthquake. Strike= 173, Dip= 60, Rake= 110. Receiver response= RSNY (sp). Azimuth= 335.

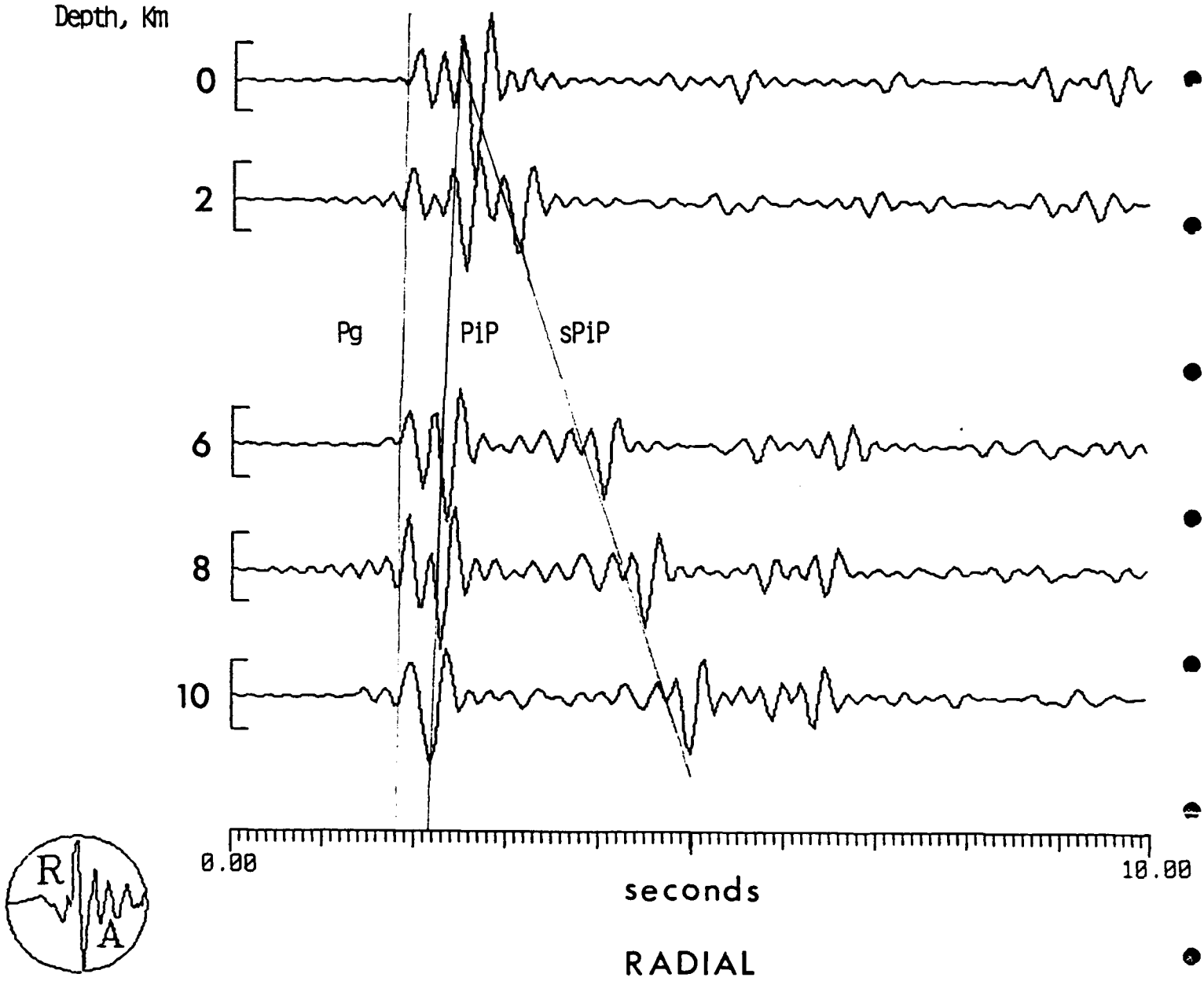

Figure 3G. Synthetic Seismogram depth section. Source= 19 October 1985 Earthquake. Strike= 022, Dip= 90, Rake= 180. Receiver response= SRNY. Azimuth= 344. Radial components shown.

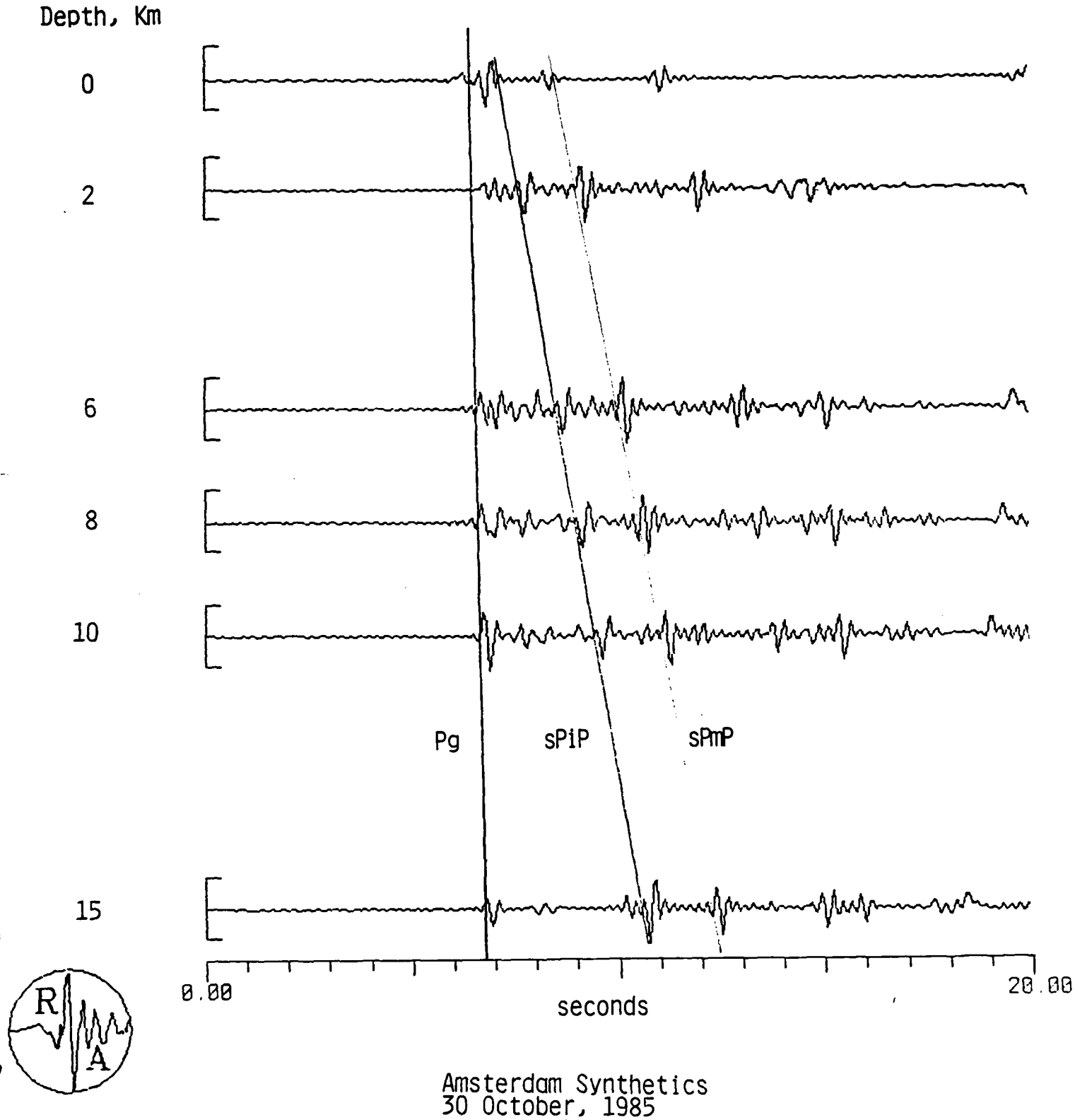

Figure 3H. Synthetic Seismogram depth section. Source at zero depth= 2 October, 1985 Explosion. Source at other depths= 30 October, 1985 Earthquake. Strike= 18, Dip= 60, Rake= 156. Receiver response= SRNY. Azimuth= 180 from explosion and 181 from Earthquake. The blast and earthquake epicenters are only 3 km apart.

TABLE 2. VELOCITY/Q MODELS

New England Model (Taylor *et al.*, 1980)

Thickness	V_P	V_S	ρ	Q_α	Q_β
2	6.0	3.5	2.5	$\frac{9}{5}Q_\beta$	$250f^{0.2}$
13	6.1	3.6	2.6		$500f^{0.2}$
25	7.0	4.1	2.9		$1000f^{0.2}$
	8.1	4.7	3.2		$3000f^{0.2}$

Grenville Model

Thickness	V_P	V_S	ρ	Q_α	Q_β
4	6.1	3.5	2.5	$1100+150\,f$	$\frac{5}{9}Q_\alpha$
31	6.6	3.7	2.7		
	8.1	4.6	3.2		

SECTION V

ANALYSIS OF JANUARY 19, 1982 NEW HAMPSHIRE EARTHQUAKE

The success of determining focal depth using depth phases and comparing them to synthetics depends largely on:

(1) good approximations of crustal velocity structure

(2) recovery and correct identification of the phases in the data.

In this section we use one earthquake to illustrate how the synthetic seismograms are affected by 2 different velocity models and focal mechanisms as well as to illustrate our approach to identifying depth phases.

Influence of some Input Parameters on Synthetics

The earthquake chosen is the Gaza, N.H., magnitude 4.5 event of January 19, 1982. Since the source is in the Appalachian Province and the receiver (RSNY) is in the Grenville Province (see Figure 1) we calculated separate synthetics using the two velocity models (Table 2) to test which is more appropriate.

Figure 4 shows radial and vertical components for the initial 15 seconds of the synthetic seismograms calculated for two velocity models. RSNY is the theoretical receiver, a distance of 267 km and an azimuth of 295^{o} from the New Hampshire source. The velocity models and Moho reflections are shown schematically for comparison. The focal mechanism is given by: strike = 280^{o}, dip = 75^{o} and rake = -11^{o}. The input focal depths are comparable.

As expected, the prominent phases and their arrival times are different for the two different velocity models. The *Pn* phase is nodal for the radiation pattern, despite small differences in take-off angles for the two models. It is simply indicated at the appropriate arrival time. For the New England model, *PmP* is small relative to *sPmP*. They both arrive before the intra-crustal reflections *PiP* and *sPiP*. For depths greater than 10 km, however, *PiP* arrives before *sPmP* (see figure 3A). *PiP* and *sPiP* are sharp arrivals because of the large velocity contrast at 15 km in the crustal model. *Vp* increases from 6.1 km/sec to 7.0 km/sec at this boundary.

For the Grenville model, *Pg* precedes the Moho reflections (for a source depth of 7 km). The amplitude of *sPmP* relative to *PmP* is smaller for the Grenville model than for the New England model because the upgoing *sPmP* is crossing a fairly sharp internal discontinuity near the source while the downgoing *PmP* only crosses this boundary once, near the receiver. In the case of New England structure, the sharp discontinuity is below the source, instead of above it. In addition, *PmP* is close to a nodal plane and small differences in take-off angle, resulting from differences in the velocity structures, may be contributing to the difference in the amplitudes of *PmP*.

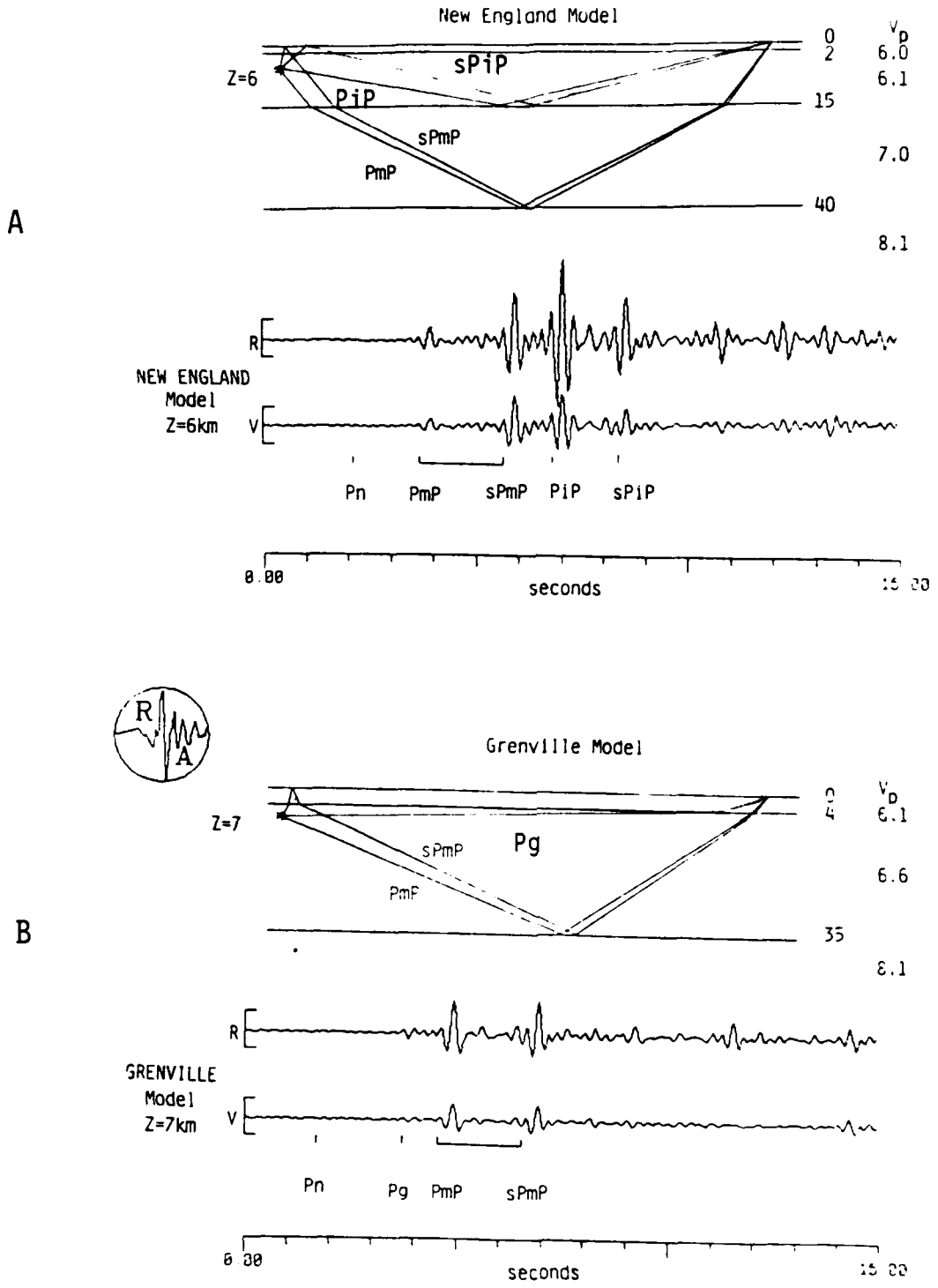

January 19, 1982, Δ= 267 Km, Azimuth= 295.

Figure 4. Two velocity models and resulting synthetic seismograms.

A= New England Model, source depth= 6 Km. Source-to-receiver Moho, reflections shown schematically. 15 seconds of radial and vertical component synthetics with phases identified. PiP and sPiP are internal reflections at the 15 Km boundary.

B= Grenville model, source depth= 7 Km. Source-to-receiver Moho reflections shown schematically. 15 seconds of radial and vertical component synthetics with phases identified.

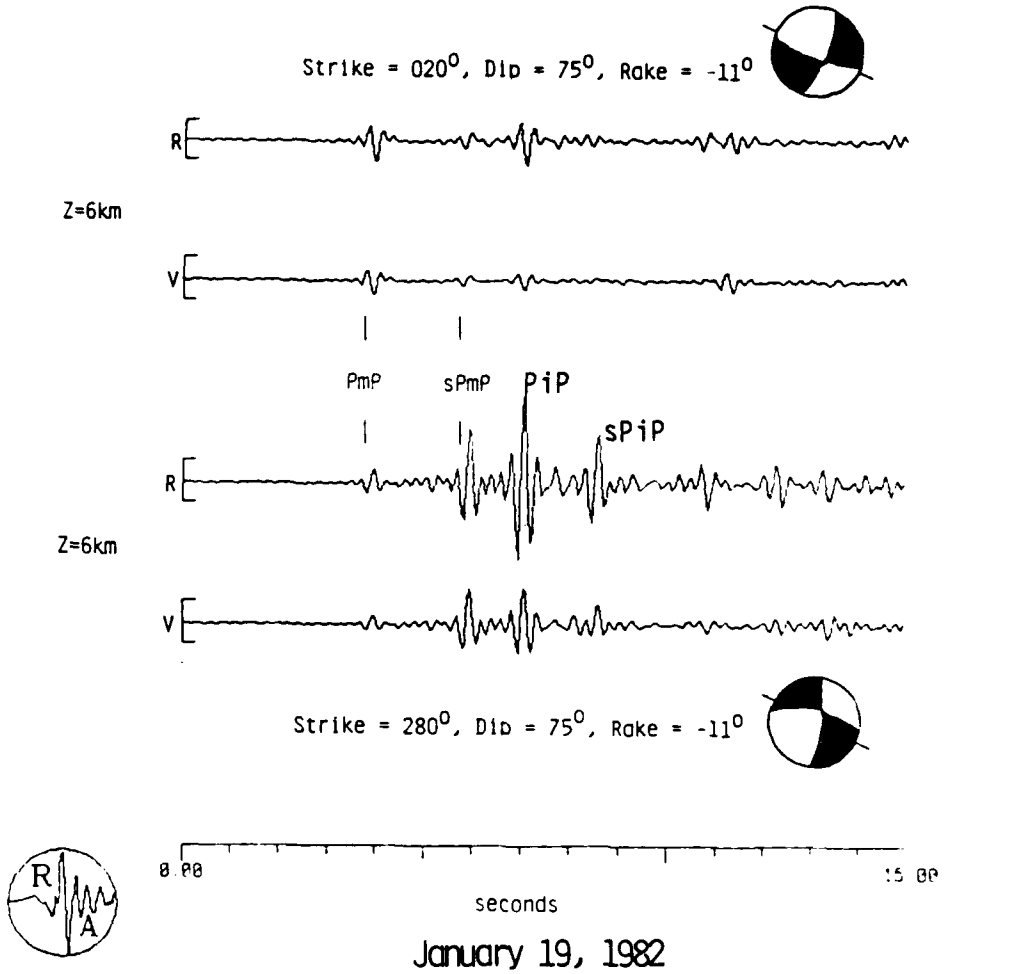

Figure 5. Two fault plane solutions and resulting synthetic seismograms. Fifteen seconds of the radial and vertical components are shown for each of the two different input solutions. The azimuth to RSNY is indicated by a line on the fault plane solution, a lower hemisphere projection with compressional quadrants filled in.

Even though the two velocity models produce strikingly different synthetic seismograms, it is important to note that for the depths and models shown, the time between the arrivals of the downgoing and upgoing Moho reflections is the same. Thus, if one can independently identify these two phases in the actual data, a match (ignoring absolute travel times) to the Grenville synthetic would suggest a depth of 7 km and a match to the New England synthetic would suggest a depth of 6 km. Given this time difference between the two arrivals, the choice of velocity model has had only a small effect on depth determination. If, however, one uses the computed phase travel times to help identify depth phases in the real data, the variation in travel time with velocity model could lead to misinterpretations of the real data.

Next, in Figure 5 we show 15 seconds of synthetics calculated for 2 different focal mechanisms. The mechanism shown at the bottom was determined from *P*-wave first motion data, mainly from the Northeast United States Seismic Network (Pulli *et al.*, 1983). The mechanism at the top of the figure differs mainly in the quadrants of dilatation and compression. The azimuth to station RSNY is very close to a nodal plane in both instances, so there is not a great difference in radiation pattern. Thus, the same initial phases appear on both sets of seismograms, but the amplitudes of these phases are different. If theoretical radiation patterns can be used to predict actual phases in the data, then it will be helpful to have independently determined fault plane solutions.

Comparison of Data to Synthetics

It would be very difficult to compare the raw data recorded at RSNY to the synthetic seismograms (compare the top of figure 2A with the synthetics in figure 3A). With the polarization filtering, however, we have been able to recover polarized phases (bottom of figure 2A) that were all but lost in the *P*-coda of the unfiltered seismograms. After polarization filtering, we low-pass filter the data to remove frequencies greater than 5 Hz, which are not modeled by the synthetics.

The following figures show comparisons of the vertical-component RSNY processed data to the vertical-component synthetic depth section calculated for the New England model. Twenty seconds are shown. We began by inserting the data at a depth of about 9 km (Figure 6). There are several arrivals in the data that match predicted arrivals. These are, in order, *PmP*, *sPmP*, the dual arrivals *PiP* and *Pg*, and finally an upgoing phase arriving toward the end of this time window. Clearly, the match is not perfect. Signal arrives in the data later than the appropriate time for *sPiP*, and, subsequently until the late phase (in the data, about 14 seconds after the initial *P*), there is not a good correlation between data and synthetics. A comparison of travel times for the first arriving phase in the data and synthetics suggests that they may not be the same phase. The travel time of synthetic *PmP* at a source depth of 9 km (with the given input velocity model) is 40.40 seconds, whereas the travel time of the first phase in the data is 38.59 seconds. Allowing for uncertainties in the actual origin time of the earthquake and for uncertainties in crustal structure, they could be the same phase. If, however, we assume that the origin time and velocity model are appropriate, we can match several early *P*-phases by aligning the data at a depth of approximately 4 1/2 km as illustrated

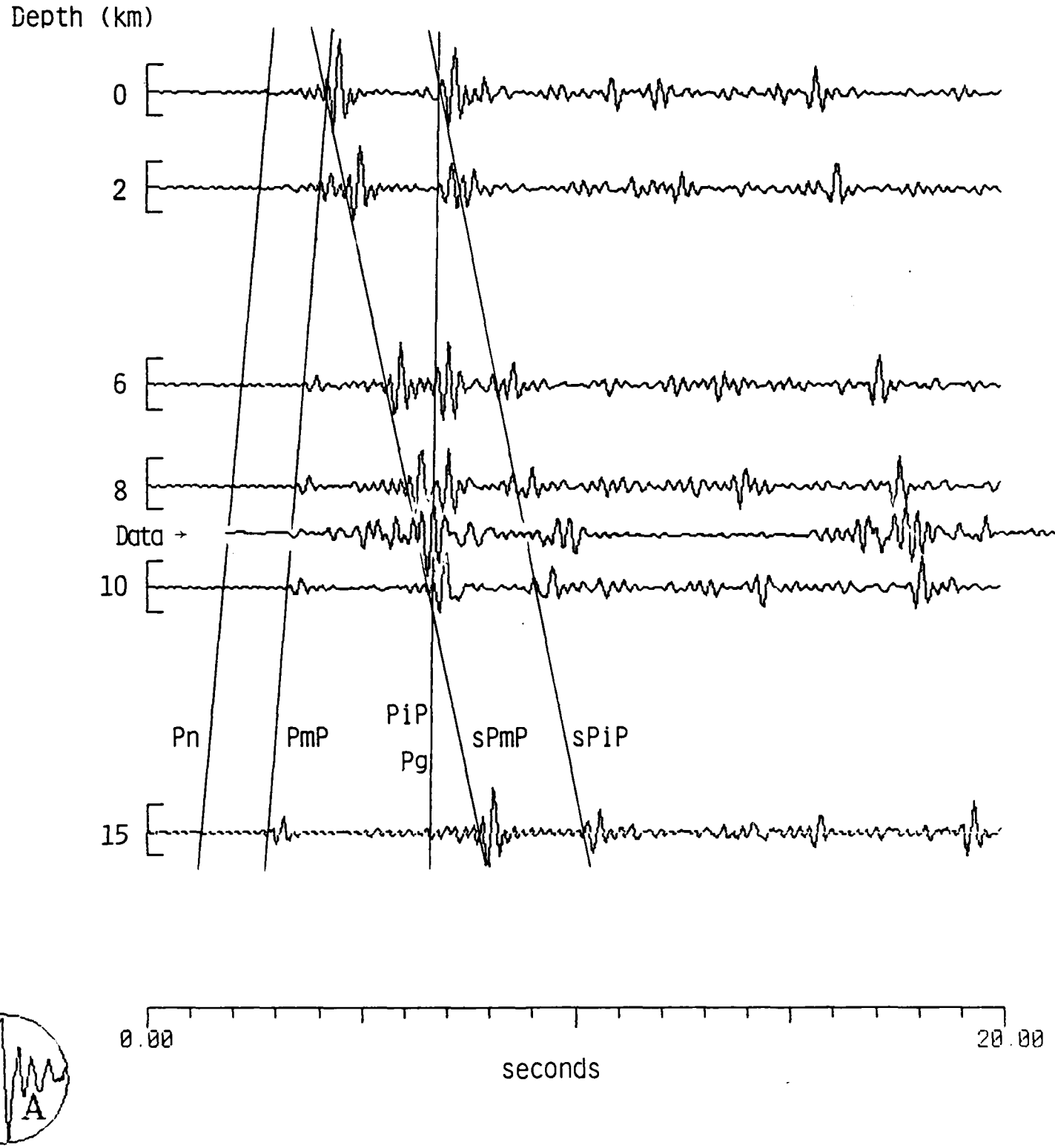

January 19, 1982
Gaza, New Hampshire
Vertical Component Synthetics
New England Velocity Model
Δ= 267 Km

Figure 6. New Hampshire earthquake, synthetic with data. Same as Figure 3A except the real Data are included in the depth section at a depth of about 9 Km. See text for discussion.

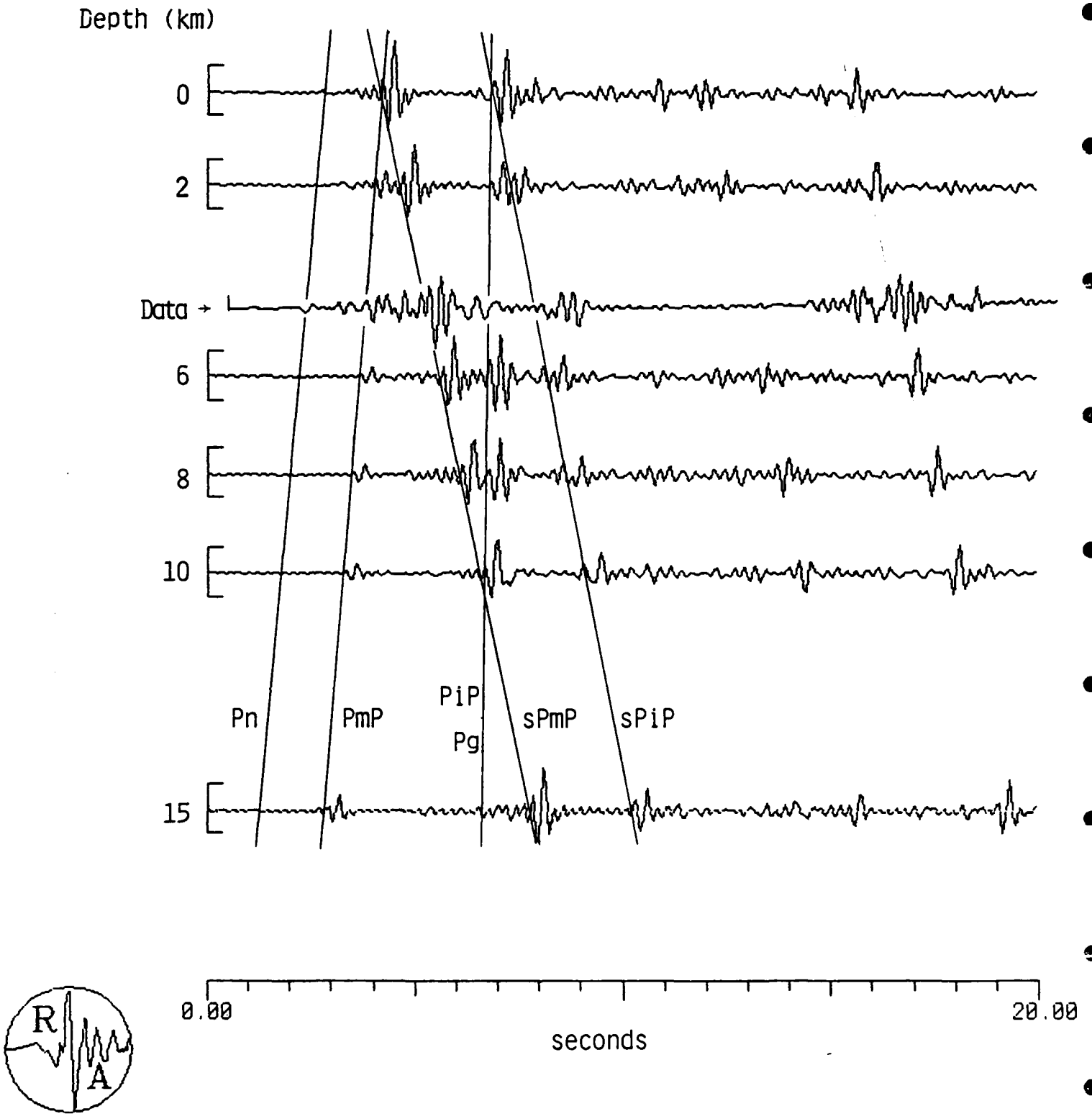

Figure 7. New Hampshire earthquake, synthetics with data. Like Figure 6 except notice that the real data are plotted at a depth of about 4.5 Km. See text for discussion.

in Figure 7. Since the real-data travel time is more appropriate for *Pn*, the first arrival is now aligned with the predicted *Pn* arrival time (compare Figures 6 and 7). For this shallower depth, the data match predicted arrival times for *Pn*,*PmP*,*sPmP* and for the late up-going phase. Again, the correlation is not perfect.

At this point, it is clear that a great deal depends on the correct identification of the arrivals in the data. In addition to travel times, the azimuth and apparent angles of incidence can be used to help identify phases. In Figure 8 we show the results of an adaptive polarization analysis of the first 20 seconds of the same state-filtered seismograms that we have been comparing to the synthetics. The first three traces in the figure are the vertical, and the adaptive radial, and transverse horizontal components. The direction of maximum signal strength as a function of time represented by the azimuth and apparent angle of incidence, is indicated (with error estimates) below the RZ product trace in Figure 8. The positive values for the product of the radial and vertical components indicate that all the phases are arriving at the receiver as *P*-waves. An adaptive polarization analysis of the synthetic seismograms indicated the same thing; thus, at the very least, we know that the last conversions were to *P*-waves for both the real and synthetic data.

Interestingly, we noted that the last arrival, which had matched a predicted phase in the synthetics at both the 4.5 and 9 km depth positions, is probably not even modeled by the synthetics. Though highly polarized and hence a prominent phase, it is fourteen degrees off the correct azimuth from the source. Unlike the two other out-of-line azimuths (see Figure 8), the error estimate does not allow enough uncertainty to put it in line. Furthermore, this late phase is approaching the receiver at a shallower angle than any other arrival (see the apparent angles of incidence), yet the late phase in the synthetic seismograms was approaching the receiver at the steepest angle in the same 20 second time window. A steep, late arrival would be consistent with a multiply-reflected phase.

The phase immediately proceeding the last phase (by almost 1 second) is more consistent with the synthetics because that phase is approaching at a steeper angle. Using that approach, a good match is obtained by inserting the data at a depth of 6 km (Figure 9). Here, the first arrival is a predicted *PmP* and there are phases matching the predicted *sPmP* and the dual arrival of *Pg* and *PiP*, as well as the late multiply-reflected phase. In addition, the relative amplitudes match the synthetics fairly well.

We have illustrated some of the difficulties in identifying and correlating depth phases from a single set of 3-component data. Evidently, this particular earthquake is difficult to pin down as the range of estimates for its focal depth is 3-11 km, using a variety of approaches (see Table 3).

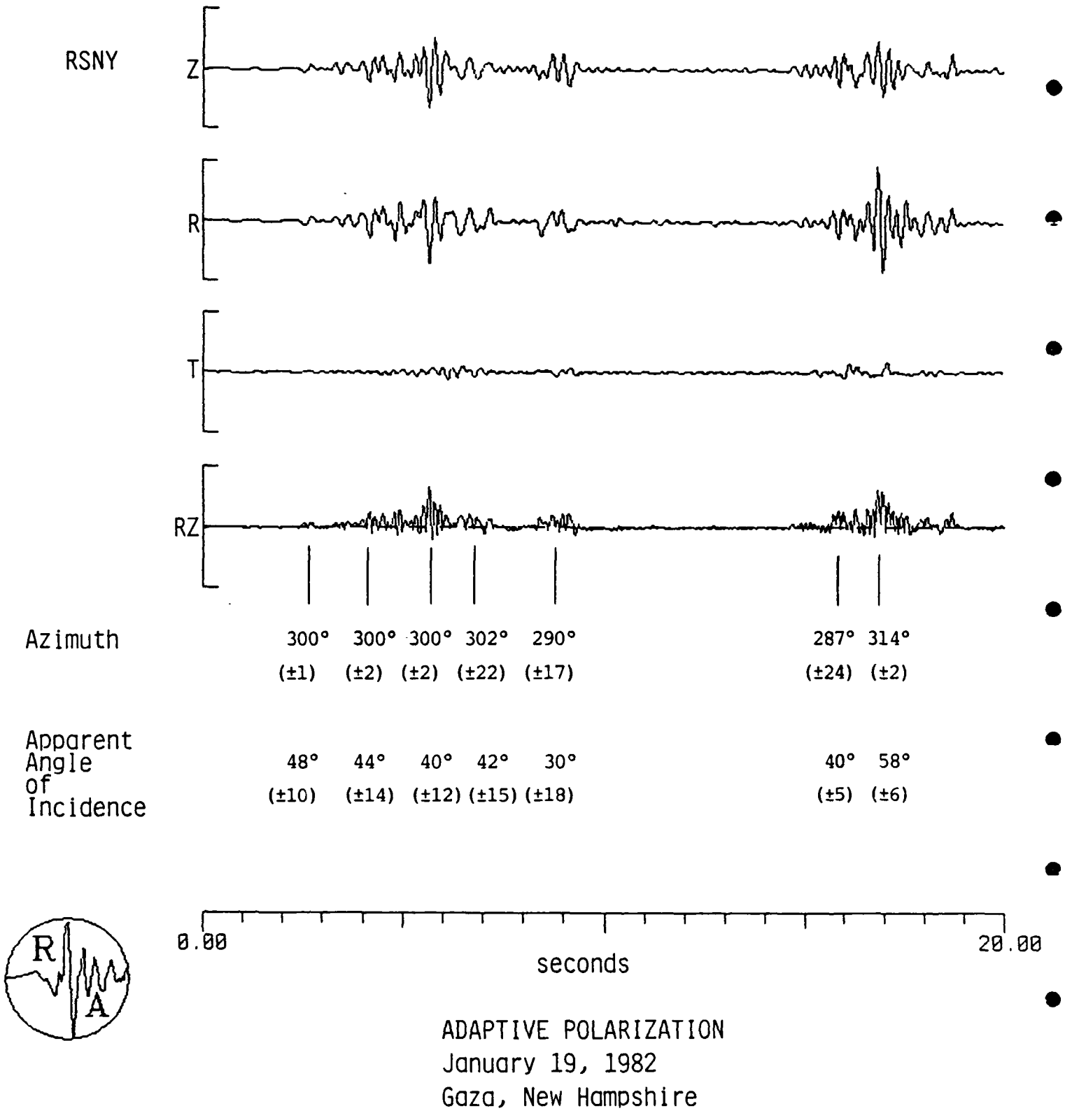

Figure 8. Adaptive polarization of state-filtered seismogram recorded at RSNY. The values of azimuth and apparent angle of incidence are given with estimated errors.

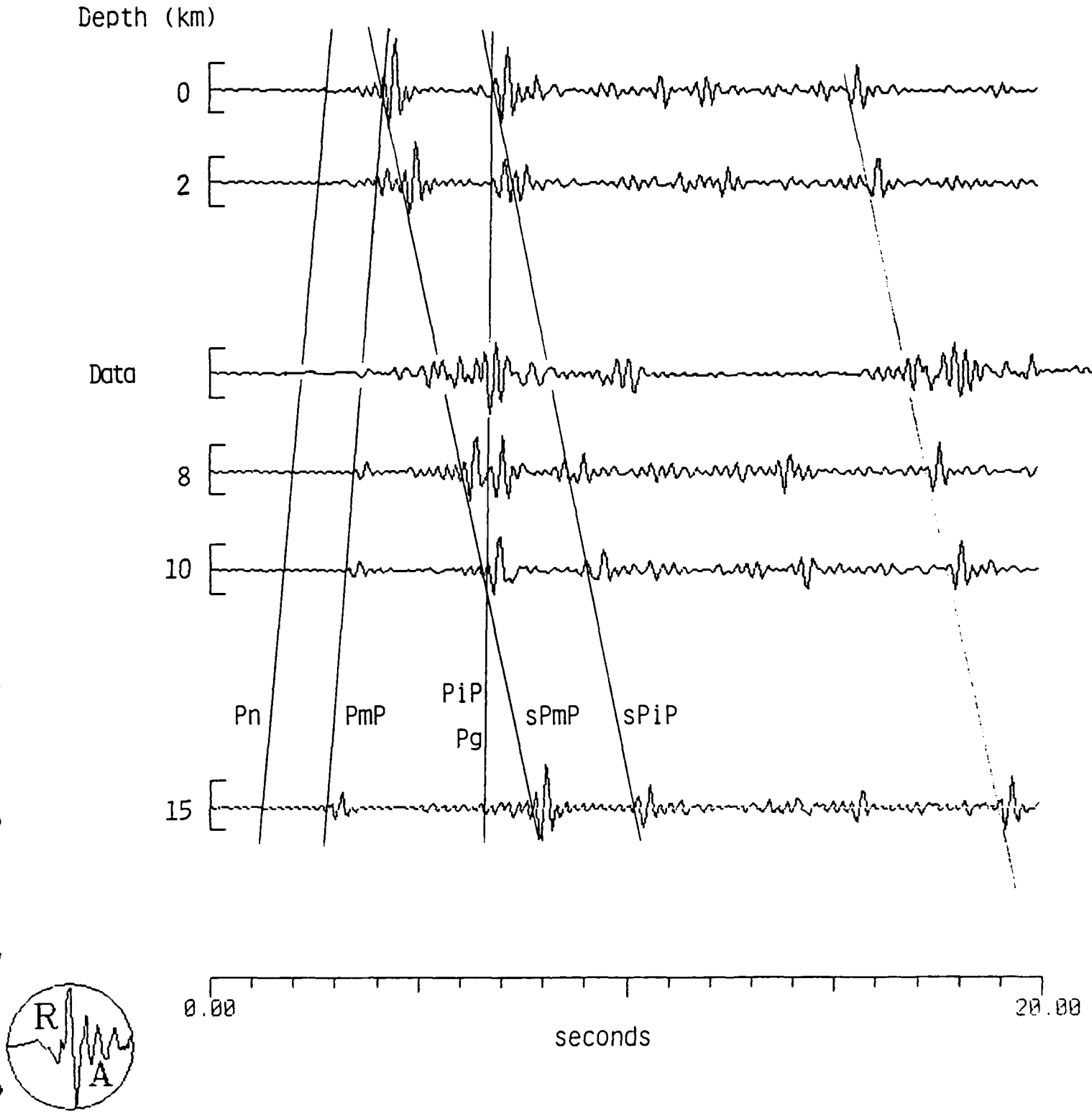

January 19, 1982
Gaza, New Hampshire
Vertical Component Synthetics
New England Velocity Model
Δ= 267 Km

Figure 9. New Hampshire earthquake, synthetics with data. Like Figures 6 and 7 except the real data are plotted at a depth of 6 Km in the depth section. See text for discussion.

TABLE 3. DEPTH ESTIMATES FOR THE GAZA, NEW HAMPSHIRE, EARTHQUAKE JANUARY 19, 1982

Depth Estimate (km)	Method	Reference
3	local network	Pulli *et al.*, 1983
3.5	teleseismic body wave modeling	Pulli *et al.*, 1983
9	relative relocations using aftershocks*	Brown and Ebel, 1985
4-11	regional, surface wave modeling	Hermann, pers. Communication

*Depth range of larger aftershocks recorded by portable instruments is 2.7-4.7km.

SECTION VI

FUTURE WORK

The work presented in this report represents the first years' research of a two year project. The major portion of the seismogram synthesis has been completed and in the months ahead only minor changes to the focal mechanisms may be necessary for the depth section.

We will continue the detailed comparisons of state-filtered and adaptively polarized data to the synthetic depth sections presented here. In addition, preliminary analysis of focal depths will be performed for several earthquakes in the Kuril/Kamchatka region. Based on the analysis in northeast United States and in Kuril/Kamchatka region, we can begin to assess the effectiveness of these approaches for depth determination. We will evaluate the recovery and identification of regional phases as well as the theoretical modeling of regional phases.

REFERENCES

Archambeau, C.B., J.C. Bradford, P.W. Broome, W.C. Dean, E.A. Flinn, and R.L. Sax, 1965, Data Processing Techniques for the Detection and Interpretation of Teleseismic Signals, Proc. IEEE, 53, 1860-1884.

Barstow, N.L., J.A. Carter and A. Suteau-Henson, 1986, Focal depths of shallow local earthquakes from comparison of polarization filtered data with synthetics, abstr. Earthquake Notes, vol. 57, No. 1, p.18.

Brown, E.J. and J.E. Ebel, 1985, An investigation of the January 1982 Aftershock Sequence near Laconia, New Hampshire, submitted to Earthquake Notes, 1985

Ebel, J.E. and J.P. McCaffrey, S.J., 1984, Hypocentral parameters and focal mechanisms of the 1983 Earthquake near Dixfield, Maine, Earthquake Notes, vol. 55, No. 2, p.21-24.

Harvey, D., 1981, Seismogram Synthetics Using Normal Mode Superposition: the Locked Mode Approximation Method, Geophys. J. Roy. Astr. Soc., 66, 37-69.

Houlday, M., R. Quittmeyer, K. Mrotek, and C.T. Statton, 1984, Recent Seismicity in North and east-central New York State, Earthquake Notes, vol. 55, No. 2, p.16-24.

Mitchell, B.J., 1981, Regional Variation and Frequency Dependence on Q_β in the Crust of the United States, Bull. Seism. Soc. Am., vol. 71, No. 5, p. 1531-1538.

Preliminary Determinations of Epicenters, Monthly listing, National Earthquake Information Center of the U.S. Geological Survey, U.S. Department of the Interior.

Pulli, J.J., J.C. Nabelek, J.M. Sauber, 1983, Source Parameters of the January 19, 1982 Gaza, New Hampshire earthquake, abst. Earthquake Notes vol. 54, No. 3, p.28-29.

Regional Seismicity Bulletin of the Lamont-Doherty Seismic Network, Lamont-Doherty Geological Observatory Publication, prepared by Schlesinger-Miller E., N. Barstow and D. Coyle.

Samson, J.C., 1977, Matrix and Stokes Vector Representations of Detectors for Polarized Waveforms: Theory with some Applications to Teleseismic Waves,

Geophys. J. Roy. Astr. Soc., 51, 583-603.

Samson, J.C. and J.V. Olson, 1981, Data-Adaptive Polarization Filters for Multichannel Geophysical Data, Geophysics, 46, 1423-1431. Publication, prepared by

Seeber, L., E.. Cranswick, N. Barstow, J. Armbruster, G. Suarez, K. Coles, and C. Aviles, 1984a, Grenville Structure and the Central Adirondack seismic zone including the October 7, 1983 Mainshock-Aftershock Sequence Canadian Geophysical Union Meeting, Halifax, Nova Scotia.

Seeber, L., E. Cranswick, J. Armbruster, and N. Barstow, 1984b, The October 1983 Goodnow, N.Y. Aftershock Sequence; Regional Seismicity and Structural features in the Adirondacks AGU abstr. 65, No. 16, p.239.

Seeber, L., J.G. Armbruster and D. Coyle, 1986, A prolonged, but spatially concentrated earthquake sequence at the northern outskirts of New York City, abstr. SSA, Earthquake Notes, vol. 57, No. 1, p.18.

Suarez G., L. Seeber, C. Aviles, and E. Schlesinger, 1984, The Goodnow, N.Y. Earthquake: Results of a Broad Band Teleseismic Analysis, AGU abstr. vol. 65, No. 16, p.239.

Sutton, G.H. and P.W. Pomeroy, 1963, Analog Analyses of Seismograms Recorded on Magnetic Tape, J. Geophys. Res., 68, 2791-2815.

Taylor, S.R., M.N. Toksoz and M.P. Chaplin, 1980, Crustal Structure of the Northeastern United States: Contrasts between Grenville and Appalachian Provinces, Science, vol. 208, p. 595-597.

Wahstrom, R., The North Gower, Ontario, Earthquake of 11 October, 1983; Focal Mechanism and Aftershocks, submitted to Earthquake Notes October 1985.

White, J.E., 1964, Motion Product Seismograms, Geophys., 29, 288-298.

DISTRIBUTION LIST
DARPA-FUNDED PROJECTS
(UNCLASSIFIED REPORTS)
(Last Revised: 3 Sep 1985)

RECIPIENT	NUMBER OF COPIES
DEPARTMENT OF DEFENSE	
DARPA/GSD 1400 Wilson Boulevard Arlington, VA 22209	2
DARPA/PM 1400 Wilson Boulevard Arlington, VA 22209	1
Defense Intelligence Agency Directorate for Scientific and Technical Intelligence Washington, D.C. 20301	1
Defense Nuclear Agency Shock Physics Directorate/SS Washington, D.C. 20305	1
Defense Technical Information Center Cameron Station Alexandria, VA 22314	12
DEPARTMENT OF THE AIR FORCE	
AFGL/LW ATTN: Dr. J. Cipar Terrestrial Sciences Division Hanscom AFB, MA 01730	1
AFOSR/NPG ATTN: Director Bldg 410, Room C222 Bolling AFB, Washington D.C. 20332	1
AFTAC/CA (STINFO) Patrick AFB, FL 32925-6441	1
AFTAC/TG Patrick AFB, FL 32925-6471	4
AFWL/NTESC Kirtland AFB, NM 87171	1

DEPARTMENT OF THE NAVY

NORDA 1
ATTN: Dr. J. A. Ballard
Code 543
NSTL Station, MS 39529

DEPARTMENT OF ENERGY

Department of Energy 1
ATTN: Dr. R. Ewing (DP-52)
International Security Affairs
1000 Independence Avenue
Washington, D.C. 20545

Lawrence Livermore National Laboratory 2
ATTN: Dr. J. Hannon and Dr. M. Nordyke
University of California
P.O. Box 808
Livermore, CA 94550

Los Alamos Scientific Laboratory 1
ATTN: Dr. K. Olsen
P.O. Box 1663
Los Alamos, NM 87544

Sandia Laboratories 1
ATTN: Mr. P. Stokes
Geosciences Department 1255
Albuquerque, NM 87115

OTHER GOVERNMENT AGENCIES

Central Intelligence Agency 1
ATTN: Dr. L. Turnbull
OSI/NED, Room 5G48
Washington, D.C. 20505

U. S. Arms Control and Disarmament Agency 1
ATTN: Dr M. Eimer
Verification and Intelligence Bureau, Rm 4953
Washington, D.C. 20451

U. S. Arms Control and Disarmament Agency 1
ATTN: Mrs. M. Hoinkes
Multilateral Affairs Bureau, Rm 5499
Washington, D.C. 20451

U.S. Geological Survey 1
ATTN: Dr. T. Hanks
Naticnal Earthquake Research Center
345 Middlefield Road
Menlo Park, CA 94025

U.S. Geological Survey 1
ATTN: Dr. R. Masse
Global Seismclogy Branch
Box 25046, Stop 967
Denver Federal Center
Denver, CO 80225

UNIVERSITIES

University of California, Berkeley 1
ATTN: Dr. T. McEvilly
Department of Geolcgy and Geophysics
Berkeley, CA 94720

California Institute of Technology 1
ATTN: Dr. D. Harkrider
Seismological Laboratory
Pasadena, CA 91125

University of California, San Diego 1
ATTN: Dr. J. Orcutt
Scripps Institute of Oceancgraphy
La Jolla, CA 92093

Columbia University 1
ATTN: Dr. L. Sykes
Lamont-Doherty Geological Observatory
Palisades, NY 10964

Massachusetts Institute of Technology 3
ATTN: Dr. S. Soloman, Dr. N. Toksoz, Dr. T. Jordan
Department of Earth and Planetary Sciences
Cambridge, MA 02139

The Pennsylvania State University 1
ATTN: Dr. S. Alexander
Department of Mineral Sciences
University Park, PN 16802

Southern Methodist University 1
ATTN: Dr. E. Herrin
Geophysical Laboratory
Dallas, TX 75275

CIRES 1
ATTN: Dr. C. Archambeau
University of Colorado
Boulder, CO 80309

St. Louis University 1
ATTN: Dr. O. Nuttli
Department of Earth and Atmospheric Sciences
3507 Laclede
St. Louis, MO 63156

DEPARTMENT OF DEFENSE CONTRACTORS

Applied Research Associates, Inc. 1
ATTN: Dr. N. Higgins
2101 San Pedro Boulevard North East
Suite A
Albuquerque, NM 87110

Applied Theory, Inc. 1
ATTN: Dr. J. Trulio
930 South La Brea Avenue
Suite 2
Los Angeles, CA 90036

Center for Seismic Studies 2
ATTN: Dr. C. Romney and Mr. R. Perez
1300 N. 17th Street, Suite 1450
Arlington, VA 22209

ENSCO, Inc. 1
ATTN: Mr. G. Young
5400 Port Royal Road
Springfield, VA 22151

ENSCO, Inc. 1
ATTN: Dr. R. Kemerait
1930 Highway A1A
Indian Harbour Beach, FL 32937

Pacific Sierra Research Corp. 1
ATTN: Mr. F. Thomas
12340 Santa Monica Boulevard
Los Angeles, CA 90025

R&D Associates 1
ATTN: Dr. E. Martinelli
P.O. Box 9695
Marina del Rey, CA 90291

Rockwell International 1
ATTN: Dr. B. Tittmann
109 Camino Dos Rios
Thousand Oaks, CA 91360

Gould Inc. 1
ATTN: Mr. R. J. Woodard
Chesapeake Instrument Division
6711 Baymeado Drive
Glen Burnie, MD 21061

Rondout Associates, Inc. 1
ATTN: Dr. P. Pomercy
P.O. Box 224
Stone Ridge, NY 12484

Science Applications, Inc. 1
ATTN: Dr. T. Bache
P.O. Box 2351
La Jolla, CA 92038

Science Horizons
ATTN: Dr. T. Cherry and Dr. J. Minster 2
710 Encinitas Blvd
Suite 101
Encinitas, CA 92024

Sierra Geophysics, Inc. 2
ATTN: Dr. R. Hart and Dr. G. Mellman
15446 Bell-Red Road
Redmond, WA 98052

SRI International 1
Attn: Dr. A. Florence
333 Ravensworth Avenue
Menlo Park, CA 94025

S-Cubed, A Division of
Maxwell Laboratories Inc.
ATTN: Dr. S. Day
P.O. Box 1620
La Jolla, CA 92038 — 1

S-Cubed, A Division of
Maxwell Laboratories Inc.
ATTN: Mr. J. Murphy
11800 Sunrise Valley Drive
Suite 1212
Reston, VA 22091 — 1

Teledyne Geotech
ATTN: Dr. Z. Der and Mr. W. Rivers
314 Montgomery Street
Alexandria, VA 22314 — 2

Woodward-Clyde Consulants
ATTN: Dr. L. Burdick
556 El Dorado St
Pasadena, CA 91105 — 1

Weidlinger Associates
ATTN: Dr. J. Isenberg
620 Hansen Way #100
Palo Alto, CA 94304 — 1

NON-US RECIPIENTS

National Defense Research Institute
ATTN: Dr. Ola Dahlman
Stockholm 80, Sweden — 1

Blacknest Seismological Center
ATTN: Mr. Peter Marshall
Atomic Weapons Research Establishment
UK Ministry of Defense
Brimpton, Reading RG7-4RS
United Kingdom — 1

NTNF NORSAR
ATTN: Dr. Frode Ringdal
P.O. Box 51
N-2007 Kjeller
Norway — 1

OTHER DISTRIBUTION

To be determined by the project office — 9